Catalytic activity of the Bin3/MEPCE methyltransferase domain is dispensable for 7SK snRNP function in *Drosophila melanogaster*

Ryan J Palumbo, Steven D Hanes

Department of Biochemistry & Molecular Biology, SUNY Upstate Medical University

750 East Adams Street, 4283 Weiskotten Hall, Syracuse, New York, 13210

PalumboR@upstate.edu, HanesS@upstate.edu

Unexpected *in vivo* results with Bin3

Keywords: Bin3, Bmc1, Bcdin3, MEPCE, Mepcea, 7SK, P-TEFb, RNA Polymerase II, Promoter-Proximal Pausing, Transcription Elongation

ABSTRACT

Methylphosphate Capping Enzyme (MEPCE) monomethylates the gamma phosphate at the 5' end of the 7SK noncoding RNA, a modification thought to protect 7SK from degradation. 7SK serves as a scaffold for assembly of a snRNP complex that inhibits transcription by sequestering the positive elongation factor P-TEFb. While much is known about the biochemical activity of MEPCE *in vitro*, little is known about its functions *in vivo*, or what roles— if any—there are for regions outside the conserved methyltransferase domain. Here, we investigated the role of Bin3, the *Drosophila* ortholog of MEPCE, and its conserved functional domains in *Drosophila* development. We found that *bin3* mutant females had strongly reduced rates of egg-laying, which was rescued by genetic reduction of P-TEFb activity, suggesting that Bin3 promotes fecundity by repressing P-TEFb. *bin3* mutants also exhibited neuromuscular defects, analogous to a patient with *MEPCE* haploinsufficiency. These defects were also rescued by genetic reduction of P-TEFb activity, suggesting that Bin3 and MEPCE have conserved roles in promoting neuromuscular function by repressing P-TEFb. Unexpectedly, we found that a Bin3 catalytic mutant (Bin3^{Y795A}) could still bind and stabilize 7SK and rescue all *bin3* mutant phenotypes, indicating that Bin3 catalytic activity is dispensable for 7SK stability and snRNP function *in vivo*. Finally, we identified a metazoan-specific motif (MSM) outside of the methyltransferase domain and generated mutant flies lacking this motif (Bin3$^{\Delta MSM}$). Bin3$^{\Delta MSM}$ mutant flies exhibited some—but not all—*bin3* mutant phenotypes, suggesting that the MSM is required for a 7SK-independent, tissue-specific function of Bin3.

33 **INTRODUCTION**

34 Regulation of eukaryotic RNA polymerase II (RNAPII) occurs at multiple stages of the
35 transcription cycle, including RNAPII recruitment to promoters by enhancer binding proteins, the
36 establishment of the pre-initiation complex, and promoter release. In higher eukaryotes an additional
37 mechanism, promoter-proximal pausing, has been shown to be critical for RNAPII regulation in
38 development and in response to signaling events (Margaritis and Holstege 2008; Gilmour 2009; Chiba
39 *et al.* 2010; Levine 2011; Li and Gilmour 2011; Nechaev and Adelman 2011; Adelman and Lis 2012; Zhou
40 *et al.* 2012; Gaertner and Zeitlinger 2014; Jonkers and Lis 2015; Liu *et al.* 2015; Mayer *et al.* 2017; Chen *et*
41 *al.* 2018; Core and Adelman 2019; Dollinger and Gilmour 2021; Gonzalez *et al.* 2021; Abuhashem *et al.*
42 2022). Pausing occurs when RNAPII stalls after transcribing approximately 30-60 nucleotides, and is
43 induced by the binding of negative elongation factors (Yamaguchi *et al.* 1999; Wang *et al.* 2010) and by
44 hypo-phosphorylation of serine 2 (Ser2) in the heptad repeat (YSPTSPS) of the carboxy-terminal
45 domain of the large subunit of RNAPII (reviewed in Brookes and Pombo 2009). Promoter proximal
46 pausing is relieved by the kinase activity of Positive Transcription Elongation Factor b (P-TEFb; Marshall
47 and Price 1995), which is a heterodimer composed of Cyclin-dependent kinase 9 (Cdk9; Marshall *et al.*
48 1996) and the regulatory cyclin, Cyclin T (CycT; Peng *et al.* 1998). P-TEFb phosphorylates negative
49 elongation factors (Wada *et al.* 1998; Cheng and Price 2007) and Ser2 (Zhou *et al.* 2000; Ramanathan *et*
50 *al.* 2001; Shim *et al.* 2002; Ni *et al.* 2004), which allows RNAPII to enter productive elongation (Ni *et al.*
51 2008).

52 To maintain a balance between transcription elongation and pausing, P-TEFb activity is highly
53 regulated; without this regulation, P-TEFb becomes "hyper-activated" and induces aberrant
54 transcription elongation (Schneeberger *et al.* 2019). Key to this regulation is the 7SK snRNP, which
55 sequesters (and thereby represses) P-TEFb (Nguyen *et al.* 2001; Yang *et al.* 2001). The "core" 7SK
56 snRNP is composed of the 7SK noncoding RNA, which acts as a scaffold for the proteins

57 Methylphosphate Capping Enzyme (MEPCE) and La-Related Protein 7 (LARP7) (Krueger *et al.* 2008;
58 Barboric *et al.* 2009; Xue *et al.* 2010; Muniz *et al.* 2013; Brogie and Price 2017; Yang *et al.* 2022). MEPCE
59 and LARP7 protect the 5' and 3' ends of 7SK from exoribonucleolytic degradation, respectively
60 (Jeronimo *et al.* 2007; Markert *et al.* 2008; Barboric *et al.* 2009; Xue *et al.* 2010; Muniz *et al.* 2013). After
61 formation of the core snRNP, 7SK RNA is reversibly bound by a homodimer of Hexamethylene Bis-
62 Acetamide Inducible Protein (HEXIM) (Blazek *et al.* 2005; Li *et al.* 2005). Binding of HEXIM to 7SK
63 induces a conformational change that allows HEXIM to bind to P-TEFb (Michels *et al.* 2004),
64 functionally sequestering and inactivating P-TEFb (Yik *et al.* 2004). Upon cellular stress and other
65 cellular signals (reviewed in Liu *et al.* 2015), binding of accessory proteins to 7SK (Herreweghe *et al.*
66 2007; Barrandon *et al.* 2007; Krueger *et al.* 2008; Lemieux *et al.* 2015; Bugai *et al.* 2019) and a
67 concomitant conformational change in the secondary structure of 7SK RNA (Krueger *et al.* 2010; Yang
68 *et al.* 2022) releases P-TEFb from the repressive 7SK snRNP. P-TEFb is then able to relieve pausing to
69 enable transcription elongation.
70 MEPCE is the long sought-after RNA methyltransferase that uses the methyl donor S-adenosyl-
71 *L*-methionine (SAM) to add a monomethyl cap to the gamma phosphate on the 5' end of 7SK (Gupta *et*
72 *al.* 1990a; Shumyatsky *et al.* 1990; Shimba and Reddy 1994), an RNA polymerase III transcript (Zieve
73 and Penman 1976; Murphy *et al.* 1986, 1987, 1989; Shumyatsky *et al.* 1990). MEPCE is human ortholog
74 of Bin3, a *Drosophila* protein that is the founding member of the Bin3/MEPCE/Bmc1 family of RNA
75 methyltransferases (Zhu and Hanes 2000; Jeronimo *et al.* 2007; Barboric *et al.* 2009; Cosgrove *et al.*
76 2012; Páez-Moscoso *et al.* 2022; Porat *et al.* 2022). We originally discovered Bin3 as an interacting
77 partner of the Bicoid homeodomain protein (Zhu and Hanes 2000). Bicoid acts as both an activator of
78 zygotic gene transcription, and a translational repressor of maternal *caudal* mRNA during
79 embryogenesis; both functions are critical for anterior-posterior patterning (Dubnau and Struhl 1996;
80 Rivera-Pomar *et al.* 1996; Chan and Struhl 1997; Niessing *et al.* 1999, 2000, 2002; Cho *et al.* 2005). We

81 had hypothesized that Bin3 was an arginine methyltransferase that methylated Bicoid to alter its
82 function, transitioning Bicoid from being a transcriptional activator to a translational repressor, or vice
83 versa. However, identification and characterization of MEPCE in human cells (originally called BCDIN3)
84 demonstrated that it is actually an RNA methyltransferase that targets 7SK to form a snRNP that
85 represses transcription (Jeronimo *et al.* 2007). We later showed that early in *Drosophila* embryogenesis,
86 Bin3 stabilizes 7SK to form a novel snRNP containing Bin3 and Bicoid (and potentially other
87 translational factors) that represses translation of maternal *caudal* mRNA at the anterior of the embryo
88 (Singh *et al.* 2011). It is important to note that Bicoid is an insect-specific protein, and therefore, the
89 translational repression function of Bin3 is also likely to be insect-specific. The canonical role of
90 Bin3/MEPCE in regulating transcription elongation, and the importance of this regulation to normal
91 development, has not been extensively studied in *Drosophila* or in other model organisms (see below).
92 Much of what we know about the 7SK RNA binding and capping functions of MEPCE comes
93 from *in vitro* or cell culture-based studies focusing on the methyltransferase activity of MEPCE and the
94 stepwise assembly of the 7SK snRNP. The monomethyl cap is believed to protect the 5' end of 7SK
95 from exoribonucleolytic degradation (Shumyatsky *et al.* 1993). However, MEPCE is peculiar in that
96 unlike most enzymes, it remains bound to the product of the reaction it catalyzes, calling into question
97 the essentiality of methyl capping. MEPCE that is constitutively bound to capped 7SK facilitates the
98 stable binding of LARP7 (Xue *et al.* 2010) to form the core 7SK snRNP (Muniz *et al.* 2013). Several
99 residues in the active site have been identified as being essential for binding to SAM and/or 7SK (Xue *et*
100 *al.* 2010; Shelton *et al.* 2018), and for methyltransferase activity (Yang *et al.* 2019). Pre-association of
101 MEPCE with 7SK was found to enhance the recruitment of LARP7 to 7SK and to MEPCE itself (Xue *et al.*
102 2010). However, whether methyltransferase activity is required *in vivo* for 7SK binding and stability, and
103 7SK snRNP function, has never explicitly been tested. Moreover, these studies have focused primarily
104 on the function of the methyltransferase domain. During evolution, MEPCE orthologs have acquired

105 extensive protein sequence flanking the methyltransferase domain, the conservation and function(s) of
106 which have not been explored.

107 Underscoring the need to understand the function of MEPCE *in vivo*, there is a
108 neurodevelopmental disorder that is caused by heterozygosity for a nonsense mutation in *MEPCE* that
109 results in P-TEFb hyper-activation (Schneeberger *et al.* 2019). However, our ability to study the *in vivo*
110 function of MEPCE and its orthologs is limited by the fact that MEPCE function appears to be essential
111 in vertebrate model organisms. For example, transfecting HeLa cells with siRNAs to destabilize 7SK
112 (which phenocopies the destabilization of 7SK in the absence of MEPCE function) results in apoptosis
113 (Haaland *et al.* 2005); treating zebrafish embryos with morpholino oligonucleotides targeting *mepcea*
114 (the zebrafish ortholog of *MEPCE*; originally named *bcdin3*) is embryonic lethal (Barboric *et al.* 2009),
115 precluding the ability to study Mepcea function in adult zebrafish; and deleting 7SK in mice (which also
116 phenocopies the destabilization of 7SK in the absence of MEPCE function) is lethal (Xu *et al.* 2022),
117 precluding the ability to study MEPCE function in adult mice. However, deleting *bin3* (the *Drosophila*
118 ortholog of *MEPCE*) does not affect the viability of adult *Drosophila* (Singh *et al.* 2011). Therefore,
119 *Drosophila* Bin3 provides a model to study the *in vivo* functions of MEPCE in metazoan development.

120 Here, we investigated the role of Bin3 in *Drosophila* development. We found that Bin3 is
121 required for fecundity and has a conserved role in promoting neuromuscular function, by repressing P-
122 TEFb. Unexpectedly, we found that Bin3 catalytic activity is dispensable for 7SK stability and snRNP
123 function *in vivo*, challenging the paradigm that methyl capping is essential for 7SK stability. Finally, we
124 identified a metazoan-specific motif (MSM) outside of the methyltransferase domain that confers a
125 7SK-independent, tissue-specific function to Bin3. These studies illustrate the importance of
126 establishing a model system in which to study this important and conserved enzyme.

127 **MATERIALS AND METHODS**

128 **Fly stocks and husbandry**

129 Fly stocks from the Bloomington *Drosophila* Stock Center (BDSC) used in this study are listed in
130 **Table S1**. Fly stocks we constructed for this study are listed in **Table S2**. The genotypes of maternal and
131 paternal flies, and the genotypes of their progeny used for experiments, and the figures in which those
132 experiments appear, are listed in **Table S3**. Fly were reared at 25°C and 60-80% humidity on a 12-hour
133 light/dark cycle, on either Nutri-Fly MF food (Genesee Scientific) with ~0.064 M propionic acid (Sigma
134 Aldrich, P5561; or Apex Bioresearch Products, 20-271), or food made based on the Nutri-Fly MF
135 formula: 25 g/L Inactive Dry Yeast (Genesee Scientific), 89.5 g/L Dry Molasses (Genesee Scientific), 57
136 g/L Fly Stuff Yellow Cornmeal (Genesee Scientific), 5.84 g/L Nutri-Fly *Drosophila* Agar, Gelidium
137 (Genesee Scientific), ~0.064 M propionic acid (Apex Bioresearch Products).

138

139 ***bin3* mutants**

140 We previously described two excision alleles that remove some ($bin3^{4\text{-}7}$) or all ($bin3^{2\text{-}7}$) of the *bin3*
141 coding exons (Parks *et al.* 2004; Singh *et al.* 2011). Both alleles were made in the same background, and
142 when placed in *trans* to produce $bin3^{4\text{-}7}/bin3^{2\text{-}7}$ mutants, incurred background effects likely due to
143 homozygosity for recessive second-site mutations. To produce *bin3* mutants that avoid these
144 confounding effects, we crossed flies heterozygous for $bin3^{2\text{-}7}$ (**Fig. 1a**) with flies heterozygous for a
145 deficiency uncovering *bin3* (*Df*, **Fig. 1a**), which is in a different genetic background than $bin3^{2\text{-}7}$ (Ryder *et*
146 *al.* 2004).

147

148 **Generation of transgenic $bin3^{+}$ rescue flies**

149 We previously showed that Bin3 is required for embryonic viability by demonstrating a *bin3* cDNA under
150 control of the maternal *Hsp83* promoter rescued the embryonic lethality of eggs laid by *bin3* mutant

151 females (Singh *et al.* 2011). To examine the role of Bin3 more broadly, we needed a rescue approach
152 that would faithfully express *bin3* under control of its own regulatory sequences in all *bin3*-expressing
153 tissues, not just in the ovary. To do this, we used BAC clone CH322-154G8 (BACPAC Genomics) that
154 comprises a 22.065 kb fragment of chromosome 2R, containing the *bin3* P1 promoter (Singh *et al.*
155 2011), and 3 of the 4 predicted mRNA isoforms of *bin3* (*bin3-RA*, *bin3-RC*, and *bin3-RD*). This BAC was
156 inserted into the *attP* landing site on chromosome 3R in BDSC stock #9744 (y^1 w^{1118}; *PBac{y⁺-attP-*
157 *9A}VK00027*) by BestGene, Inc.
158
159 **Generation of the pUAS-DSCP-XbaI-attB vector via NEBuilder HiFi DNA Assembly**
160 High-copy plasmids pNP (Qiao *et al.* 2018; Wang *et al.* 2019) and pUASP-attB (Drosophila Genomics
161 Resource Center Stock 1358; https://dgrc.bio.indiana.edu//stock/1358; RRID:DGRC_1358; Takeo *et al.*
162 2012) were purified from bacterial cells grown to confluence at 37°C in LB + 100 µg/ml ampicillin using
163 the Monarch Plasmid Miniprep Kit T1010L from New England BioLabs, Inc. (NEB). To create pUAS-
164 DSCP-XbaI-attB (the vector into which *bin3* and 3xHA sequences would be cloned, see below), the
165 10XUAS-DSCP promoter was amplified from plasmid pNP with Q5 High-Fidelity DNA Polymerase
166 (NEB) using primers UP0394 and UP0395, and inserted into pUASP-attB that had been digested with
167 *Xho*I (NEB) and *Pst*I (NEB), via NEBuilder HiFi DNA Assembly (NEB.). NEBuilder HiFi DNA Assembly
168 destroyed the *Xho*I site, and partially eliminated one of the two GAGA enhancers in pUASp-attB .
169
170 **Ovarian RNA Purification and Reverse Transcription for NEBuilder HiFi DNA Assembly**
171 one to three-day old w^{1118} (BDSC #5905) females were incubated with males in yeasted vials overnight.
172 Five pairs of ovaries were dissected from two to four-day old females in ice-cold 1X PBS, and flash-
173 frozen in liquid nitrogen. Total RNA was extracted using the Monarch Total RNA Miniprep Kit (NEB),
174 according to the manufacturer's instructions for RNA purification from "Tissues". Total RNA (1 µg) was

175 reverse transcribed using ProtoScript II First Strand cDNA Synthesis Kit (NEB, E6560S) with primer
176 UP0118, which anneals to the very end of *bin3* coding sequence (CDS). See **Table S4** for primer
177 sequence.
178
179 **Purification of BAC clone CH322-154G8 for NEBuilder HiFi DNA Assembly**
180 EPI300 bacterial cells (Lucigen) harboring the BAC clone CH322-154G8 (BACPAC Genomics) were
181 grown to confluence at 37°C in LB + 12.5 µg/ml chloramphenicol, and plasmid replication was induced
182 by diluting 1:10 in LB + 12.5 µl/ml chloramphenicol and 1X CopyControl Induction Solution (Lucigen).
183 The BAC was purified purified using the Monarch Plasmid Miniprep Kit (NEB).
184
185 **Generation of *UAS-DSCP-3xHA-bin3* transgenic flies via NEBuilder HiFi DNA Assembly**
186 To generate plasmid *pUAS-DSCP-3xHA-bin3-attB*, which expresses Bin3 C-terminally tagged with 3xHA,
187 under UAS control: Fragment #1, comprising the *bin3-RA* 5' -UTR to the end of the *bin3* CDS, was
188 amplified from *bin3* cDNA using Q5 High-Fidelity DNA Polymerase, and primers UP0423 and UP0414.
189 The 5' end of Fragment #1 is homologous to sequences immediately upstream of the *Xba*I site in
190 pUAS-DSCP-XbaI-attB; the 3' end of Fragment #1 is homologous to 5' end of a synthetic dsDNA
191 fragment comprising Gly-Gly-Gly-Ser-3xHA (G_4S-3xHA; Integrated DNA Technologies) codon-
192 optimized for *Drosophila* with the IDT Codon Optimization Tool (Integrated DNA Technologies).
193 Fragment #2, comprising the entire *bin3-RA* 3' -UTR, was amplified from the BAC clone CH322-154G8
194 using Q5 High-Fidelity DNA Polymerase, and primers UP0415 and UP0424. The 5' end of Fragment #2
195 is homologous to the 3' end of the G_4S-3xHA fragment; the 3' end of Fragment #2 is homologous to
196 sequences immediately downstream of the *Xba*I site in pUAS-DSCP-XbaI-attB. Fragment #1, G_4S-
197 3xHA, and Fragment #2 were assembled in this order into the *Xba*I site of pUAS-DSCP-XbaI-attB via
198 NEBuilder HiFi DNA Assembly. The *Xba*I site was destroyed.

199

200 To generate plasmid *pUAS-DSCP-3xHA-bin3*^{Y795A}*-attB*, which expresses catalytically-dead Bin3^{Y795A}, C-
201 terminally tagged with 3xHA ,under UAS control: Fragment #3, comprising the *bin3-RA* 5' -UTR to 11 nt
202 downstream of the Y795 codon, was amplified from *bin3* cDNA using Q5 High-Fidelity DNA
203 Polymerase, and primer UP0423 and the mutagenic primer UP0419, which introduces a Y795A point
204 mutation. The 5' end of Fragment #3 is homologous to sequences immediately upstream of the *Xba*I
205 site in pUAS-DSCP-XbaI-attB; the 3' end of Fragment #3 is homologous to the 5' end of Fragment #4.
206 Fragment #4, comprising 11 nt upstream of the Y795 codon to the end of the *bin3-RA* CDS was
207 amplified from cDNA using Q5 High-Fidelity DNA Polymerase, and mutagenic primer UP0420, which
208 introduces a Y795A point mutation, and primer UP0414. The 5' end of Fragment #4 is homologous to
209 the 3' end of Fragment #3; the 3' end of Fragment #4 is homologous to 5' end of the G_4S-3xHA
210 fragment. Fragment #3, Fragment #4, G_4S-3xHA, and Fragment #2 (see above) were assembled in this
211 order into the *Xba*I site of pUAS-DSCP-XbaI-attB via NEBuilder HiFi DNA Assembly. The *Xba*I site was
212 destroyed.
213

214 To generate plasmid *pUAS-DSCP-3xHA-bin3*$^{\Delta MSM}$*-attB*, which expresses Bin3$^{\Delta MSM}$, C-terminally tagged
215 with 3xHA, under UAS control: Fragment #5, comprising the *bin3-RA* 5' -UTR to 12 nt downstream of
216 the L326 codon, was amplified from *bin3* cDNA using Q5 High-Fidelity DNA Polymerase, and primer
217 UP0423 and the mutagenic primer UP0417, which eliminates codons 311-326. The 5' end of Fragment
218 #5 is homologous to sequences immediately upstream of the *Xba*I site in pUAS-DSCP-XbaI-attB; the 3'
219 end of Fragment #5 is homologous to the 5' end of Fragment #6. Fragment #6, comprising 12 nt
220 upstream of the F311 codon to the end of the *bin3-RA* CDS was amplified from cDNA using Q5 High-
221 Fidelity DNA Polymerase and mutagenic primer UP0418, which eliminates codons 311-326, and primer
222 UP0414. The 5' end of Fragment #6 is homologous to the 3' end of Fragment #5; the 3' end of

223 Fragment #6 is homologous to 5' end of the G_4S-3xHA fragment. Fragment #5, Fragment #6, G_4S-
224 3xHA, and Fragment #2 (see above) were assembled in this order into the *Xba*I site of pUAS-DSCP-
225 XbaI-attB via NEBuilder HiFi DNA Assembly. The *Xba*I site was destroyed.
226
227 See **Table S4** for primer sequences and the sequence of the G_4S-3xHA synthetic dsDNA fragment used
228 to make these 3 constructs. Sequencing of each construct revealed that all UTRs corresponded to the
229 *bin3-RA* mRNA isoform of *bin3*. Interestingly, each construct had an in-frame insertion of an Ala residue
230 between L573 and V574, when mapped to the reference sequence of *bin3* (NCBI Reference Sequence
231 NM_165468.2). These 3 constructs were recombined into the *attP* landing site on chromosome 3L in
232 BDSC stock #8622 (y^1 w^{67c23}; $P\{y^{+t7.7}$=*CaryP*}*attP2*) by BestGene, Inc.
233
234 **Expression of *UAS-DSCP-3xHA-bin3* transgenes using the Trojan GAL4 approach**
235 We used the UAS/GAL4 system (Brand and Perrimon 1993) and the Trojan GAL4 approach (Diao and
236 White 2012; Diao *et al.* 2015; Lee *et al.* 2018) to induce the expression of *UAS-DSCP-3xHA-bin3* (hereon
237 referred to as *UAS-bin3*) transgenes. Intronic Trojan GAL4 insertions produce a null allele of a gene
238 while also expressing GAL4 under the regulatory sequences of that gene. A Trojan GAL4 insertion into
239 one of the *bin3* introns ($bin3^{MI08045\text{-}TG4.0}$, hereon referred to as $bin3^{TG4.0}$) in *trans* to a deficiency (*Df*)
240 uncovering *bin3* produces *bin3*-null ($bin3^{TG4.0}/Df$) flies that express GAL4 in the spatiotemporal pattern of
241 endogenous *bin3*. (**Fig. 4a**). When transgenes comprising *UAS-bin3* cDNAs (**Fig. 5d-f**) are incorporated
242 into $bin3^{TG4.0}/Df$ flies, GAL4 induces expression of Bin3 proteins in the pattern of endogenous *bin3* in an
243 otherwise *bin3*-null background.
244
245 **Total RNA purification from ovaries and RT-qPCR**

246 Five one to three-day old females were incubated with males in yeasted vials overnight. Five pairs of
247 ovaries were dissected from two to four-day old females in ice-cold 1X PBS, and flash-frozen in liquid
248 nitrogen. Total RNA was extracted using the Monarch Total RNA Miniprep Kit (NEB), according to the
249 manufacturer's instructions for RNA purification from "Tissues". RT-qPCR was performed on 10 ng total
250 RNA using the Luna Universal One-Step RT-qPCR Kit (NEB, E3005L). *bin3*, 7SK, U6, and *rp49* mRNAs
251 were reverse transcribed and amplified with primers UP0493 + UP0118, UP0146 + UP0147, OW1123 +
252 OW1124, and UP0113 + UP0114, respectively (see **Table S4** for primer sequences). Reactions were
253 performed using a CFX Opus 384 Real-Time PCR System (Bio-Rad).
254
255 **Protein extraction and Western Analysis**
256 Ten one to three-day old females were incubated with males in yeasted vials overnight. Ten pairs of
257 ovaries were dissected from two to four-day old females in ice-cold 1X PBS, and flash-frozen in liquid
258 nitrogen. Protein was exacted as previously described {Prudêncio.2015}. Extracts were clarified through
259 0.22 µM Spin-X columns (Costar), and mixed 1:1 with 2X Sample Loading Buffer (Bio-Rad) + 5% β-
260 mercaptoethanol, and boiled for 5 minutes. Extracts were spun down, and 15 µl was loaded onto 4-20%
261 TGX gels (Bio-Rad), and ran at 100 V for 10 minutes, then 300 V for 20 minutes. Protein was transferred
262 to PVDF-LF membranes (Bio-Rad) using a Trans-Blot Turbo Transfer System (Bio-Rad) using the High
263 MW preset (1.3 A, 25 V, 10 minutes). Membranes were blocked in EveryBlot Blocking Buffer (Bio-Rad)
264 for 5 minutes, and then incubated with primary antibodies diluted in EveryBlot Blocking Buffer for 1
265 hour at room temperature. Membranes were washed with TBST (1X Tris-Buffered Saline, 0.2% Tween-
266 20) for 5 minutes 3 times, and then incubated with secondary antibodies diluted in EveryBlot Blocking
267 Buffer for 1 hour at room temperature. Membranes were with TBST for 5 minutes 3 times, dehydrated
268 with 100% methanol, and imaged using a ChemiDoc MP Imaging System with Image Lab Touch
269 software (Bio-Rad). Primary antibodies used were 1 µg/ml rabbit anti-HA (abcam, ab9110), and 1 µg/ml

270 mouse anti-beta Actin (abcam, ab170325), and 5 µg/ml IgG purified from sheep anti-CycT antiserum
271 (Nguyen *et al.* 2012). using Pierce Protein G Magnetic Beads according to the manufacturer's
272 instructions. Secondary antibodies were from Jackson ImmunoResearch, Inc., and used at 1 µg/ml:
273 Alexa Fluor 488 AffiniPure Donkey Anti-Rabbit IgG (711-545-152), Alexa Fluor 488 AffiniPure Donkey
274 Anti-Sheep IgG (713-545-147), Alexa Fluor 594 AffiniPure Donkey Anti-Mouse IgG (715-585-150), and
275 Alexa Fluor 647 AffiniPure Donkey Anti-Mouse IgG (715-605-150).
276
277 **Egg-Laying Assay**
278 Ten one to three-day old virgin females were incubated with wild-type males *en masse* in yeasted vials
279 overnight. Ten two to four-day old females were split individually into fresh vials with two Oregon-R
280 males, and incubated for 24 hours. After 24 hours, eggs were counted to determine the number of eggs
281 laid/female/day. Experiments were performed in biological triplicate.
282
283 **Immunofluorescence staining of ovaries**
284 Immunofluorescence staining of ovaries was performed as described (Maimon and Gilboa 2011). Ten 1-
285 4 day old females were incubated with males in yeasted vials overnight, and then 10 pairs of ovaries
286 were dissected from 2-5 day old females in ice-cold 1X PBS. The following steps were performed at RT
287 unless otherwise indicated. Ovaries were fixed in 1 ml of Image-iT Fixative Solution (Thermo Scientific,
288 R37814) + 0.3% Triton X-100 for 20 minutes. Ovaries were washed and permeabilized with 1 ml of 1% PT
289 Buffer (1X PBS, 1% Triton X-100) for 5 minutes, 10 minutes, and 45 minutes. Ovaries were blocked with
290 1 ml PBT (1X PBS, 1% BSA, 0.3% Triton X-100) for 1 hour, and then incubated in 250 µl PBT and primary
291 antibodies overnight at 4°C. Primary antibodies used were 1 µg/ml rabbit anti-HA (abcam ab9110) and 5
292 µg/ml mouse anti-Vasa (Developmental Studies Hybridoma Bank, Vasa 46F11). Ovaries were washed
293 with 1 ml 0.3% PT Buffer (1X PBS, 0.3% Triton X-100) 3 times for 30 minutes each, blocked with 1 ml

294 PBT-NDS (1X PBS, 1% BSA, 0.3% Triton X-100, 5% normal donkey serum) for 1 hour, and incubated in
295 250 µl PBT-NDS containing 10 µg/ml Hoechst 33342 (Thermo Scientific, H3570) and 2 µg/ml secondary
296 antibodies for 2 hour in the dark. Secondary antibodies were from Jackson ImmunoResearch, Inc.:
297 Alexa Fluor 488 AffiniPure Donkey Anti-Rabbit IgG (711-545-152) and Alexa Fluor 647 AffiniPure Donkey
298 Anti-Mouse IgM (715-605-020). Ovaries were washed with 1 ml 0.3% PT Buffer in the dark 3 times for 30
299 minutes each, then mounted in 50 µl VECTASHIELD PLUS Antifade Mounting Medium (Vector Labs,
300 Inc., H-1900-10).
301
302 **Single-molecule fluorescence *in situ* hybridization (smFISH) in ovaries**
303 smFISH on adult ovaries was performed essentially as described (Raj and Tyagi 2010; Abbaszadeh and
304 Gavis 2016). Ten 1-4 day old females were incubated with males in yeasted vials overnight, and then 10
305 pairs of ovaries were dissected from 2-5 day old females in ice-cold 1X PBS. The following steps were
306 performed at RT unless otherwise indicated. Ovaries were fixed in 1 ml of Image-iT Fixative Solution
307 (Thermo Scientific, R37814) for 30 minutes, then washed with PBST (1X PBS, 0.1% Tween-20) 3 times
308 for 5 minutes each. Ovaries were permeabilized by incubating in 7:3 PBST:methanol for 5 minutes, 1:1
309 PBST:methanol for 5 minutes, 3:7 PBST:methanol for 5 minutes, 100% methanol for 10 minutes, 3:7
310 PBST:methanol for 5 minutes, 1:1 PBST:methanol for 5 minutes, and 7:3 PBST:methanol for 5 minutes.
311 Ovaries were then washed with PBST 4 times for 5 minutes each, followed by pre-hybridized in Wash
312 Buffer A (20% Stellaris RNA FISH Wash Buffer A (Biosearch Technologies Cat# SMF-WA1-60) and 10%
313 deionized formamide) for 5 minutes. Ovaries were incubated in Stellaris RNA FISH Hybridization Buffer
314 (Biosearch Technologies Cat# SMF-HB1-10) with 10% deionized formamide and 125 µM Quasar 640-
315 labeled oligonucleotide probes, overnight at 37°C in the dark. Oligonucleotide probes against 7SK were
316 designed using the LGC Biosearch Technologies' Stellaris RNA FISH Probe Designer
317 (https://www.biosearchtech.com/support/tools/design-software/stellaris-probe-designer). Ovaries

318 were washed in the dark with Wash Buffer A for 30 minutes at 37°C, and then with Wash Buffer A with
319 10 µg/ml Hoechst 33342 (Thermo Scientific, H3570) for 30 minutes at 37°C, and finally with Stellaris RNA
320 FISH Wash Buffer B (Biosearch Technologies Cat# SMF-WB1-20) for 5 minutes at RT. Ovaries were
321 mounted in 50 µl VECTASHIELD PLUS Antifade Mounting Medium (Vector Labs, Inc., H-1900-10).
322
323 **Ovariole Counting Assay**
324 One to three-day old females were incubated with sibling males in yeast vials overnight. Two to four-
325 day females were anesthetized, transferred to 1.7 ml tubes, flash-frozen in liquid nitrogen, and stored at
326 -80°C. Frozen females were thawed on ice or at RT and dissected in a 1:1 mixture of methanol and 1X
327 PBS. 50% methanol dehydrates and extracts lipids from the gonadal sheath surrounding the ovary and
328 from the clear portions of the ovarioles (turning them opaque), making ovarioles easy to separate and
329 count. The mean number of ovarioles per ovary, as well as the absolute value of the difference in
330 ovariole number between each ovary per female were calculated (Lobell *et al.* 2017). Experiments were
331 performed in biological duplicate.
332
333 **Climbing Assay**
334 Ten 2-5 day old females were transferred to 15 ml tubes, and allowed to acclimate for 3'. Flies were
335 tapped to the bottom of the tube, and climbing was recorded for 12 seconds. Flies were then allowed to
336 reacclimatize for another 3 minutes before performing the subsequent trial. 10 trials were performed
337 per genotype to determine the percent of flies climbing 8 cm in 12 seconds per trial. All genotypes for a
338 particular experiment were tested at the same time. Experiments were performed in biological
339 triplicate.
340
341 **Modeling of Bin3 protein sequence onto MEPCE**

342 Bin3 was modeled onto 309 amino acids of the MEPCE active site in complex with *S*-adenosyl-*L*-
343 homocysteine (SAH) and stem loop 1 of 7SK (PDB 6dcb; Yang *et al.* 2019) using hhpred (Söding 2005;
344 Hildebrand *et al.* 2009; Meier and Söding 2015; Zimmermann *et al.* 2018; Gabler *et al.* 2020) and
345 MODELLER (Šali *et al.* 1995; Zimmermann *et al.* 2018; Gabler *et al.* 2020). Alignment of the Bin3 model
346 to 6dcb, RMSD calculation, and modeling of the Y421A and Y795A mutations was performed using
347 PyMol (version 2.5.4).
348
349 **Bin3 Disorder Prediction**
350 Disorder in Bin3 was predicted by IUPred3, using the IUPred3 short disorder analysis type (Mészáros *et*
351 *al.* 2018; Erdős and Dosztányi 2020; Erdős *et al.* 2021).
352
353 **RNA Immunoprecipitation (RIP)**
354 Twenty-five one to three-day old females with or without transgenes expressing *bin3-3xHA* cDNAs
355 were incubated with males in yeasted vials overnight. Twenty-five pairs of ovaries were dissected from
356 two to four-day old females in ice-cold, 1X PBS, and fixed in 1 ml 1.8% formaldehyde (a mixture of 55%
357 1X PBS and 45% Image-iT Fixative Solution, Thermo Scientific, R37814) for 15 minutes at RT on a
358 nutating rotor. Fixation was terminated by addition of 163 µl 2.5 M glycine to a final concentration of
359 ~350 mM, and incubation for 5 minutes at RT on a nutating rotor. Ovaries were washed briefly with with
360 1X PBS 3 TIMES, and then flash-frozen in liquid nitrogen. Ovaries were homogenized by hand with a
361 blue pestle on ice in 50 µl ice-cold RIPA Lysis and Extraction Buffer (Thermo Scientific, 89900)
362 supplemented with 1 mM DTT, 3X Halt Protease and Phosphatase Inhibitor Cocktail (Thermo Scientific,
363 78440), and 1 U/µl SUPERase•In RNase Inhibitor (Invitrogen, AM2696). 200 µl of additional buffer was
364 added to the homogenate, and samples were incubated on ice for 15 minutes to allow for complete
365 nuclear lysis. Homogenate was pelleted by centrifugation at top speed for 1 minute. 2.5 µl of

366 homogenate (1/100th homogenate volume) was removed and kept on ice in a total of 300 µl 1X Monarch
367 DNA/RNA Protection Reagent (NEB, T2011L) as the input sample. The remaining homogenate was
368 used for immunoprecipitation. 25 µl (1/10th homogenate volume) of Pierce Anti-HA Magnetic Beads
369 (Thermo Scientific, 88836) were washed with 175 µl 1X TBS-T (Pierce 20X TBS Tween 20 Buffer,
370 Thermo Scientific, 28360), and then with 1 ml 1X TBS-T. Homogenate was added to the washed beads,
371 and immunoprecipitation was performed for 4 hours at 4°C with end-over-end rotation. Beads were
372 washed briefly with 1 ml 1X TBS-T 3 times. Bin3-3xHA complexes were purified by two sequential
373 competitive elutions with 75 µl of Pierce HA Peptide (Thermo Scientific, 26184) diluted to 2 mg/ml in
374 Nuclease-Free Water (NEB, B1500L), at 37°C for 15 minutes each. The eluates were pooled, and the 150
375 µl total eluate was added to 150 µl 2X Monarch DNA/RNA Protection Reagent. All samples (inputs and
376 eluates) were incubated at 65-70°C for 30 minutes to reverse formaldehyde crosslinks. Total RNA was
377 extracted using the Monarch Total RNA Miniprep Kit (NEB), according to the manufacturer's
378 instructions for RNA purification from "Tissues". Total RNA was eluted in 100 µl Nuclease-Free Water.
379 2.9 µl of each sample was used in 10-µl reactions to reverse transcribe and amplify 7SK and U6 snRNAs
380 with primers UP0146 + UP0147 and OW1123 + OW1124, respectively (see **Table S4** for primer
381 sequences). Reactions were performed using the Luna Universal One-Step RT-qPCR Kit (NEB, E3005L)
382 and a CFX Opus 384 Real-Time PCR System (Bio-Rad).

383 **RESULTS**

384 **Bin3 is required for female fecundity**

385 Reproductive success is influenced by fertility (offspring viability) and fecundity (the rate of
386 offspring production). Previously, we showed that Bin3 plays a role in fertility, promoting embryonic
387 viability by a mechanism of *caudal* translation repression (Singh *et al.* 2011). During that and other
388 studies, we noticed that *bin3* mutants lay fewer eggs than wild type flies. Therefore, we asked if Bin3
389 also plays a role in fecundity by promoting a normal egg-laying rate. To do this, we compared the egg-
390 laying rates of flies that were either wild type for *bin3* (wt), heterozygous for *bin3* ($bin3^{2\text{-}7}$/+), or deleted
391 entirely for *bin3* ($bin3^{2\text{-}7}$ in *trans* to a deficiency that removes the *bin3* locus; $bin3^{2\text{-}7}/Df$). The genomic
392 regions deleted by $bin3^{2\text{-}7}$ and *Df* are depicted in **Fig. 1a**. As expected, *bin3* mRNA levels are reduced by
393 half in $bin3^{2\text{-}7}$/+ heterozygotes and are undetectable in $bin3^{2\text{-}7}/Df$ mutants (**Fig. 1b**). Interestingly, we
394 found that $bin3^{2\text{-}7}/Df$ females laid eggs at a significantly reduced rate compared to wt (P = .0001) and
395 $bin3^{2\text{-}7}$/+ (P < .0001) females (**Fig. 2a**). The egg-laying rate defect was specific to the loss of *bin3*, as a
396 single copy of a genomic fragment containing the *bin3* ORF ($bin3^{+}$, **Fig. 1a**) restored *bin3* mRNA
397 accumulation by half (**Fig. 1b**) and rescued the egg-laying defect of $bin3^{2\text{-}7}/Df$ females (P < .0001, **Fig.**
398 **2a**). Rescue was comparable to that of $bin3^{2\text{-}7}$/+ controls. These results demonstrate that Bin3 is
399 required for egg-laying.

400

401 **Bin3 promotes female fecundity by repressing P-TEFb**

402 We found that 7SK RNA levels were strongly reduced in $bin3^{2\text{-}7}/Df$ females compared to wt (P <
403 .0001, **Fig. 1c**), as we have previously shown (Singh *et al.* 2011). The canonical function of Bin3/MEPCE
404 is to stabilize 7SK RNA (Jeronimo *et al.* 2007; Singh *et al.* 2011). 7SK RNA in turn acts as a scaffold for
405 proteins that form a snRNP that sequesters and represses P-TEFb (Krueger *et al.* 2008; Barboric *et al.*
406 2009; Xue *et al.* 2010; Muniz *et al.* 2013; Brogie and Price 2017; Yang *et al.* 2022). Therefore,

407 destabilization of 7SK in *bin3*$^{2-7}$*/Df* females should lead to deregulation (activation) of P-TEFb, which
408 could be responsible for the egg-laying defect. If this is true, then we expect that reducing the activity
409 of P-TEFb in *bin3*$^{2-7}$*/Df* females would rescue the egg-laying defect. To genetically reduce the activity of
410 P-TEFb, we introduced a mutant allele of *CycT* (*CycT*^{llB2}) into *bin3*$^{2-7}$*/Df* flies, and confirmed that this
411 mutation reduces the protein levels of the largest of the two CycT isoforms (**Fig. 1e**). Indeed, we found
412 that reducing the amount of CycT in *bin3*$^{2-7}$*/Df* females rescued the egg-laying defect (P < .0001, **Fig.**
413 **2a**), while having no effect on 7SK RNA levels (**Fig. 1c**). These results suggest that Bin3 stabilizes 7SK
414 RNA to form the 7SK snRNP, which then sequesters and represses P-TEFb to promote a normal egg-
415 laying rate.
416
417 **Bin3 and 7SK are expressed ubiquitously in the ovary**
418 To gain insight into the role of Bin3 in egg-laying, we determined where Bin3 (and its substrate
419 7SK) is expressed and localized in ovaries, which are composed of 16-20 individual ovarioles that can be
420 thought of as assembly lines of germline development (**Fig. 2b**). We used the UAS/GAL4 (Brand and
421 Perrimon 1993) and Trojan GAL4 systems (see Materials and Methods; Diao and White 2012; Diao *et al.*
422 2015; Lee *et al.* 2018), where a Trojan GAL4 insertion into the *bin3* ORF was used to drive the expression
423 of a 3xHA-epitope-tagged *bin3* transgene in the spatiotemporal pattern of endogenous *bin3* (*bin3*$^{TG4.0}$ >
424 *UAS-3xHA-bin3*). Bin3-3xHA was detected by immunofluorescence staining of ovaries. We found that
425 Bin3 is expressed in and localized to the nucleic of all ovarian cells (**Fig. 2, c, c'**). Bin3 was found to be
426 expressed in the germline cells of the germarium (located at the anterior of each ovariole), and in the 15
427 nurse cells that supply the oocyte with mRNAs and proteins. Bin3 was also found to be expressed in the
428 somatic cells surrounding the germline cells and the oocyte, which communicate with germline cells to
429 promote egg chamber and oocyte maturation. Control flies lacking the *UAS-3xHA-bin3* transgene
430 (*bin3*$^{TG4.0}$/+) yielded no detectable HA staining (**Fig. 2, d, d'**).

431 To identify where in the ovary 7SK RNA is expressed and localized, we performed single-
432 molecule fluorescence *in situ* hybridization (Raj and Tyagi 2010; Abbaszadeh and Gavis 2016) on ovaries
433 from wt and *bin3*$^{2\text{-}7}$*/Df* females. We found that in wt ovarioles, 7SK follows an identical expression
434 pattern to that of Bin3 (compare **Fig. 2, e, e'** with **Fig. 2, c, c'**). As expected, 7SK staining was
435 undetectable in *bin3*$^{2\text{-}7}$*/Df* ovarioles (**Fig. 2, f, f'**), which do not accumulate 7SK RNA (**Fig. 1c**). Taken
436 together, Bin3 and 7SK are both expressed in all cells of the ovarioles and localize to nuclei—
437 commensurate with their role in transcription elongation regulation.
438
439 **Bin3 is not required to establish the proper number of ovarioles**
440 The total number of ovarioles per ovary directly correlates with the number of eggs insects can
441 lay (Wayne *et al.* 1997; Wayne and Mackay 1998), and is established by proper proliferation and
442 migration of the somatic terminal filament cells (TFCs; Sahut-Barnola *et al.* 1995, 1996). Given that we
443 found *bin3*$^{2\text{-}7}$*/Df* mutant females had an egg-laying defect, and that Bin3 is expressed in the somatic
444 cells of the ovarioles, we hypothesized that Bin3 promotes egg-laying by functioning in the TFCs to
445 establish ovarioles. To test this hypothesis, we used the UAS/GAL4 system (Brand and Perrimon 1993)
446 with two different *bab1-GAL4* drivers (Cabrera *et al.* 2002) to induce expression of the *UAS-3xHA-bin3*
447 transgene specifically in the somatic TFCs of *bin3*$^{2\text{-}7}$*/Df* females to determine whether this rescued the
448 egg-laying rate. Unfortunately, we were unable to recover *bin3*$^{2\text{-}7}$*/Df; bab1-GAL4/UAS-bin3* flies using
449 either driver. Both *bab1-GAL4* drivers are expressed in several cell types in addition to the TFCs (Cabrera
450 *et al.* 2002), and therefore it is likely that ectopic expression of *bin3* in all *bab1*-expressing cells is lethal.
451 As an alternative approach, we compared ovariole numbers in *bin3*$^{2\text{-}7}$*/Df* females with those of
452 wt and *bin3*$^{2\text{-}7}$/+ controls. To do this, we dissected ovaries and determined (i) the average number of
453 ovarioles per ovary, and (ii) the difference in the number of ovarioles within a pair of ovaries (i.e.,
454 "ovariole asymmetry"; Lobell *et al.* 2017). Unexpectedly, we did not find a significant difference in

455 either the mean number of ovarioles per ovary (**Fig. 2g**) or in ovariole asymmetry (**Fig. 2h**) in *bin3*$^{2\text{-}7}$*/Df*
456 females compared to either wt or *bin3*$^{2\text{-}7}$/+ control females.
457 Together, these results suggest that Bin3 is not required to establish ovarioles, and therefore
458 promotes egg-laying by some other mechanism. These results also suggest that Bin3 does not have a
459 function in TFCs relevant to the establishment of ovarioles. However, these results do not rule out some
460 other function of Bin3 in TFCs (*e.g.*, cell-cell communication with germline cells) that might promote
461 egg-laying. The lethality of inducing *bin3* expression in TFCs using the *bab1-GAL4* drivers precludes the
462 ability to test this hypothesis in any straightforward way.
463
464 **Expression of Bin3 in the germline is not sufficient to promote fecundity**
465 Bin3 is also expressed in germline cells, therefore, it remained possible that Bin3 functions in
466 the germline to promote a normal egg-laying rate. To test this hypothesis, we used a *nanos-*
467 *GAL4::VP16* driver (Doren *et al.* 1998) to induce expression of the *UAS-3xHA-bin3* transgene specifically
468 in the germline cells of *bin3*$^{2\text{-}7}$*/Df* females, and asked whether this improved the egg-laying rate (**Fig.**
469 **2g**). Results showed that germline expression of *bin3* did not rescue the egg-laying rate defect of *bin3*$^{2\text{-}}$
470 ^{7}*/Df; nanos-GAL4::VP16/UAS-bin3* females compared to *bin3*$^{2\text{-}7}$*/Df; nanos-GAL4::VP16/*+ mutant females
471 (*P* = .9942, **Fig. 2i**), suggesting that Bin3 does not function in germline cells to promote a normal egg-
472 laying rate.
473
474 **Bin3 has a conserved role in neuromuscular function**
475 A nonsense mutation in the *MEPCE* gene of a patient with impaired neuromuscular ability was
476 shown to reduce MEPCE protein levels, causing P-TEFb hyper-activation and aberrant RNAPII
477 transcription elongation (Schneeberger *et al.* 2019). If a conserved function of Bin3/MEPCE is to repress
478 P-TEFb to promote normal neurodevelopment, then it would be expected that *bin3* mutant flies would

479 also have neuromuscular defects, and that these defects should be rescued by reducing CycT levels
480 (lowering P-TEFb activity).
481 Two ways in which neuromuscular function can be assessed in flies is by examining climbing
482 (Manjila and Hasan 2018) and resting wing posture (Baehrecke 1997). Normally, flies climb to the top of
483 an enclosure after being knocked to the bottom, and fold their wings one-over-the-other when resting.
484 We found that a significant percentage of *bin3*$^{2\text{-}7}$*/Df* flies had a climbing defect compared to *bin3*$^{2\text{-}7}$/+
485 control flies (P = .0003, **Fig. 3a**). Additionally, whereas control *bin3*$^{2\text{-}7}$/+ flies properly folded their wings
486 (**Fig. 3b**), *bin3*$^{2\text{-}7}$*/Df* mutant flies had a *held-out wings* phenotype (**Fig. 3c**). Both defects were specific to
487 loss of *bin3*, as the *bin3*$^{+}$ genomic fragment rescued the climbing (*P* = .0004, **Fig. 3a**) and resting wing
488 posture defects of *bin3*$^{2\text{-}7}$*/Df* flies (compare **Fig. 3d** with **Fig. 3c**). Importantly, both climbing (*P* = .0008,
489 **Fig. 3a**) and wing posture (compare **Fig. 3e** with **Fig. 3c**) defects of *bin3*$^{2\text{-}7}$*/Df* flies were also rescued by
490 reducing CycT levels. These results suggest that Bin3 and MEPCE share a conserved role in
491 neuromuscular function from *Drosophila* to humans, most likely by repressing P-TEFb and preventing
492 aberrant transcription elongation.
493
494 **Bin3 catalytic activity is dispensable for 7SK stability and snRNP function *in vivo***
495 The importance of MEPCE catalytic residues in 7SK binding and capping have been studied
496 mostly *in vitro* (Xue *et al.* 2010; Shelton *et al.* 2018; Yang *et al.* 2019). To determine the importance of
497 Bin3 catalytic activity *in vivo,* we sought to generate flies expressing a catalytically-dead Bin3 protein.
498 We first analyzed the crystal structure of the methyltransferase domain of human MEPCE (PDB 6dcb,
499 Yang *et al.* 2019). As shown in **Fig. 4a,** Tyrosine 421 (Y421) is juxtaposed between the 5' gamma
500 phosphate of 7SK and S-adenosyl-*L*-homocysteine (SAH; used in place of the S-adenosyl-*L*-methionine
501 (SAM) methyl donor for the purposes of crystallization). Y421 hydrogen bonds to the 7SK gamma
502 phosphate. Mutation of this tyrosine to alanine (Y421A) completely abolished MEPCE catalytic activity

503 *in vitro* (Yang *et al.* 2019). We modeled Bin3 onto the crystal structure (**Fig. 4a**) and found that Y795 in
504 Bin3 (red) aligned well with Y421 in MEPCE (black). We created models (**Fig. 4b**) representing the
505 Y421A mutation in MEPCE (black) and the concomitant Y795A mutation in Bin3 (red), which revealed a
506 complete loss of coordination between 7SK, SAH (i.e., SAM), and MEPCE/Bin3.

507 Given the *in vitro* importance of the Y421 residue in MEPCE for catalytic activity, and that Y795
508 in Bin3 aligns with Y421, we generated flies expressing either wt Bin3 ($Bin3^{wt}$) or $Bin3^{Y795A}$ and tested
509 whether $Bin3^{Y795A}$ was able to (i) bind and stabilize 7SK, and (ii) rescue *bin3* mutant phenotypes. To do
510 this, we again used the Trojan GAL4 approach. Importantly, not only do Trojan GAL4 insertions express
511 GAL4 in the pattern of the gene they are inserted into, but they simultaneously generate a null allele of
512 the inserted gene. Indeed, *bin3* Trojan GAL4 insertion flies ($bin3^{TG4.0}/Df$) (**Fig. 4d**) had nearly
513 undetectable levels of both *bin3* mRNA ($P < .0001$, **Fig. 4e**) and 7SK RNA ($P < .0001$ **Fig. 4f**) compared to
514 wt, confirming that $bin3^{TG4.0}$ is a null allele of *bin3*. Additionally, we found that GAL4 expressed from
515 $bin3^{TG4.0}$ induced both $UAS\text{-}bin3^{wt}$ (**Fig. h**) and $UAS\text{-}bin3^{Y795A}$ (**Fig. 4i**) transgenes similarly at the mRNA
516 ($P = .2188$, **Fig. 4k**) and protein ($P = .9836$, **Fig. 4l**) levels. Thus, these flies could be used to study the
517 importance of Bin3 catalytic activity *in vivo*.

518 Bin3 catalytic activity is expected to be required for capping and stabilization of 7SK *in vivo*;
519 therefore, in $Bin3^{Y795A}$ mutant flies, 7SK should be destabilized. Remarkably, there was no significant
520 difference in 7SK levels between $Bin3^{Y795A}$ flies ($bin3^{TG4.0}/Df;\ UAS\text{-}bin3^{Y795A}/+$) and $Bin3^{wt}$ flies ($bin3^{TG4.0}/Df;$
521 $UAS\text{-}bin3^{wt}/+$; $P = .9996$, **Fig. 5a**), suggesting that Bin3 catalytic activity is not required for the stability
522 of 7SK *in vivo*. How then might Bin3 stabilize 7SK in the absence of catalytic activity? As suggested by
523 prior studies (Xue *et al.* 2010), Bin3 might form a stable complex with 7SK independent of its catalytic
524 function, and this may protect it from degradation. Indeed, we find that $Bin3^{Y795A}$ immunoprecipitated
525 as much 7SK RNA as did $Bin3^{wt}$ ($P = .5350$, **Fig. 5b**), suggesting that the Y795A mutation does not
526 diminish the binding of Bin3 to 7SK, and that binding alone is sufficient for stabilization *in vivo*.

527 Given that Bin3^{Y795A} could bind and stabilize 7SK, we expected that Bin3^{Y795A} would rescue the
528 fecundity, climbing, and wing posture defects of *bin3* mutant flies. First, we showed that *bin3*$^{TG4.0}$*/Df*
529 flies recapitulate the fecundity (compare **Fig. 6a** to **Fig. 2a**), climbing (compare **Fig. 6b** with **Fig. 3a**),
530 and wing posture (compare **Fig. 6d** with **Fig. 3c**) defects of *bin3*$^{2-7}$*/Df* flies. As expected, Bin3^{Y795A}
531 expression rescued the fecundity (P = .0008, **Fig. 6a**), climbing (P < .0001, **Fig. 6b**), and wing posture
532 (compare **Fig. 6f** to **Fig. 6d**) defects of *bin3*$^{TG4.0}$*/Df* flies, similar to Bin3^{wt} (P > .9999 for both fecundity
533 and climbing). Therefore, despite the importance of catalytic activity to 7SK capping *in vitro*, Bin3
534 catalytic activity and therefore the methylphosphate cap do not seem to be required *in vivo* for 7SK
535 stability, nor is it likely to affect 7SK snRNP assembly and function (**Fig. 6i**).
536
537 **A metazoan-specific motif in Bin3 is required to promote specific neuromuscular functions**
538 Much attention has been given to the methyltransferase domain of Bin3 orthologs; however,
539 metazoans have acquired over evolutionary time additional protein sequences outside of the
540 methyltransferase domain (Cosgrove *et al.* 2012). To determine whether there is conserved homology
541 between Bin3 orthologs in these regions, we aligned several Bin3 orthologs that have been previously
542 characterized, including *Drosophila* Bin3 (Zhu and Hanes 2000; Singh *et al.* 2011; Cosgrove *et al.* 2012),
543 human MEPCE (Xue *et al.* 2010; Muniz *et al.* 2013; Shelton *et al.* 2018; Schneeberger *et al.* 2019; Yang *et*
544 *al.* 2019; Lee *et al.* 2020; Zhang *et al.* 2021), zebrafish Bcdin3 (Barboric *et al.* 2009), and *S. pombe* Bmc1
545 (Páez-Moscoso *et al.* 2022; Porat *et al.* 2022). We discovered a 16-amino acid motif that is almost
546 entirely conserved in metazoans (flies, zebrafish, and humans), but is absent in the fission yeast *S.*
547 *pombe* (**Fig. 4c**). Therefore, we have named this motif the Metazoan-Specific Motif (MSM). The N-
548 terminal portion of this motif is predicted to be more structured (IUPred3 score 0.2733 to 0.3764), while
549 the C-terminal portion is predicted to be less structured (IUPred3 score 0.4062 to 0.5887). Given the
550 strong conservation of the MSM, we hypothesized that the MSM must contribute to some important

551 function of Bin3 and its metazoan orthologs. To test this hypothesis, we used the Trojan GAL4 system
552 to generate flies expressing either Bin3^{wt} or Bin3 deleted of the entire 16-aa MSM (Bin3$^{\Delta MSM}$) and asked
553 whether Bin3$^{\Delta MSM}$ could (i) bind and stabilize 7SK, and (ii) rescue *bin3* mutant phenotypes.
554 We found that GAL4 expressed from *bin3*$^{TG4.0}$ induced both the *UAS-bin3*^{wt} (**Fig. 4h**) and *UAS-*
555 *bin3*$^{\Delta MSM}$ (**Fig. 4j**) transgenes to express similar levels of mRNA (*P* = .3840, **Fig. 4k**) and protein (*P* =
556 .7994, **Fig. 4l**). Given that the MSM is outside of the Bin3 methyltransferase domain, we did not expect
557 that the Bin3 MSM would be required for 7SK stability or binding. Accordingly, there was no significant
558 difference in 7SK levels (*P* = .3846, **Fig. 5a**) between Bin3$^{\Delta MSM}$ flies (*bin3*$^{TG4.0}$*/Df; UAS-bin3*$^{\Delta MSM}$/+) and
559 Bin3^{wt} flies (*bin3*$^{TG4.0}$*/Df; UAS-bin3*^{wt}/+). Also, Bin3$^{\Delta MSM}$ immunoprecipitated as much 7SK (*P* = .9938, **Fig.**
560 **5b**) as did Bin3^{wt}.
561 Given that 7SK was bound and stabilized by Bin3$^{\Delta MSM}$, we expected that Bin3$^{\Delta MSM}$ would rescue
562 the fecundity, climbing, and wing posture defects of *bin3*$^{TG4.0}$*/Df* flies. Indeed, Bin3$^{\Delta MSM}$ expression
563 rescued the fecundity (*P* = .0061, **Fig. 6a**) and climbing (*P* < .0001) defects of *bin3*$^{TG4.0}$*/Df* flies, similar to
564 Bin3^{wt} (*P* = .6681, **Fig. 6a**; *P* = .0685, **Fig. 6b**). However, Bin3$^{\Delta MSM}$ did not rescue the *held-out wings*
565 phenotype of *bin3*$^{TG4.0}$*/Df* flies (compare **Fig. 6g** with **Fig. 6d**), suggesting that while the MSM is
566 dispensable for Bin3 function in the contexts of egg-laying and climbing, the Bin3 MSM plays a critical
567 role in normal resting wing posture, independent of 7SK (**Fig. 6i**). Interestingly, reducing CycT dosage in
568 Bin3$^{\Delta MSM}$ flies (*bin3*$^{TG4.0}$*/Df; UAS-bin3*$^{\Delta MSM}$*/CycT*^{j11B2}) rescued the *held-out wings* defect (compare **Fig. 6h**
569 with **Fig. 6g**). We think that because Bin3$^{\Delta MSM}$ binds and stabilizes 7SK (and as such, forms the 7SK
570 snRNP to repress P-TEFb; **Fig. 5b**) it is unlikely that the MSM directly contributes to P-TEFb repression;
571 instead, genetically reducing P-TEFb activity probably had a non-specific rescuing effect by globally
572 tapering transcription elongation.
573
574 **Bin3 binds to the U6 spliceosomal RNA, but is not required for its stability**

575 MEPCE in humans (Jeronimo *et al.* 2007; Muniz *et al.* 2013) and Bmc1 in *S. pombe* (Páez-
576 Moscoso *et al.* 2022; Porat *et al.* 2022) bind to the U6 spliceosomal snRNA, but are not required for U6
577 stability. We asked whether Bin3 in *Drosophila* also binds to U6 and whether Bin3 is also dispensable for
578 U6 stability.

579 We found that $Bin3^{wt}$ (P = .0113), $Bin3^{Y795A}$ (P = .0033), and $Bin3^{\Delta MSM}$ (P = .0336) all bind to U6
580 snRNA, compared to un-tagged control. We also found that there is no significant difference in the
581 amount of U6 bound by $Bin3^{Y795A}$ (P = .7671) or $Bin3^{\Delta MSM}$ (P = .8486) compared to $Bin3^{wt}$ (**Fig. 5d**). These
582 results show for the first time that Bin3 in *Drosophila* binds to U6, and that neither catalytic activity nor
583 the MSM are required for binding. It is not surprising that $Bin3^{\Delta MSM}$ binds to U6, as Bmc1 lacks this
584 region (Cosgrove *et al.* 2012), yet it binds to U6 (Páez-Moscoso *et al.* 2022; Porat *et al.* 2022). And, like
585 MEPCE and Bmc1, we found that Bin3 is not required for U6 stability. U6 levels (**Fig. 5c**) were not
586 different between flies expressing $Bin3^{wt}$ and $Bin3^{Y795A}$ (P = .8794) or $Bin3^{\Delta MSM}$ (P = .7529), and were not
587 significantly affected in $bin3^{2-7}/Df$ flies (P = .9314, **Fig. 1d**). U6 levels were reduced by approximately half
588 in $bin3^{TG4.0}/Df$ flies (P = .0471, **Fig. 4g**); however, these data were just below the threshold for
589 significance (α = 0.05). Taken together, Bmc1, Bin3, and MEPCE have a conserved function in binding to
590 the U6 snRNA, but are not required for its stability.

591 **DISCUSSION**

592 In this study, we showed that Bin3, the *Drosophila* ortholog of the 7SK methylphosphate
593 capping enzyme, MEPCE, has a conserved role in promoting normal metazoan development by
594 regulating the P-TEFb positive elongation factor (**Figs. 7a, 8a**). We further investigated Bin3 by
595 determining the *in vivo* requirement for two different regions of the Bin3 protein: the methyltransferase
596 domain, and a previously undiscovered motif that is specific to metazoan orthologs of Bin3. To our
597 surprise, we found that the catalytic activity of the methyltransferase domain appears to be
598 dispensable for the function of Bin3 as a constituent of the repressive 7SK snRNP (**Fig. 7b**). By contrast,
599 the metazoan-specific motif in Bin3 is required for a tissue-specific function, one that is 7SK-
600 independent (**Figs. 7c, 8b**). We also provide the first evidence in *Drosophila* for binding of Bin3 to the U6
601 spliceosomal snRNA. As in other model organisms (Jeronimo *et al.* 2007; Muniz *et al.* 2013; Páez-
602 Moscoso *et al.* 2022; Porat *et al.* 2022), we found that Bin3 was not required for U6 stability.
603

604 **Bin3 represses P-TEFb to promote normal fly physiology**

605 The canonical function of MEPCE is to *repress* gene expression by binding to and stabilizing 7SK
606 snRNA, which acts as a scaffold for proteins that sequester P-TEFb (Peterlin *et al.* 2011; Cosgrove *et al.*
607 2012). This inhibits P-TEFb, which normally phosphorylates RNAPII to promote transcription
608 elongation. Consequently, loss of MEPCE function destabilizes 7SK, dissociates the repressive snRNP,
609 releasing P-TEFb (Fujinaga *et al.* 2023). Hyper-activated P-TEFb induces aberrant gene expression by
610 ectopic phosphorylation of RNAPII and other factors (He *et al.* 2008; Schneeberger *et al.* 2019). A non-
611 canonical function of MEPCE is to *activate* gene expression by binding to the tail of histone H4 and
612 recruiting free P-TEFb to chromatin. This non-canonical function was found be required for the
613 induction of tumorigenic genes in a breast cancer cell line (Shelton *et al.* 2018). Here, we show that Bin3
614 contributes to normal fly physiology through a mechanism most consistent with its canonical function

615 in repression of P-TEFb. We found that the egg-laying, climbing, and wing posture defects of *bin3*
616 mutants were rescued by genetically reducing the activity of P-TEFb with a mutation in *CycT* (which is
617 needed for P-TEFb kinase activity). Thus, in fly development, Bin3 appears to repress P-TEFb (and gene
618 expression) rather than to activate P-TEFb (**Figs. 7a, 8a**).
619
620 **Bin3 is required for reproductive success**
621 Previously, we found that Bin3 plays a role in fertility by promoting embryonic viability (Singh *et*
622 *al.* 2011). Here, we show that Bin3 is required for fecundity by supporting a normal egg-laying rate (**Fig.**
623 **7a**). Thus, Bin3 has a role in two different aspects of reproductive success: fertility (offspring viability),
624 and fecundity (the rate of offspring production).
625 Although Bin3 and its substrate 7SK are expressed in all germline and somatic cells of the ovary,
626 germline expression of Bin3 was dispensable for a normal egg-laying rate. A germline function for Bin3
627 might occur later in development, consistent with our previous finding that Bin3 appears to regulate the
628 translation of *grk* in late-stage oocytes (Singh *et al.* 2011), which is important for embryonic patterning.
629 A previous report demonstrated that both wild-caught flies harboring indels in *bin3*, and
630 transgenic flies harboring transposon insertions into *bin3*, have reduced numbers of ovarioles (Lobell *et*
631 *al.* 2017). However, we found that our $bin3^{2\text{-}7}/Df$ mutant females did not exhibit reduced ovariole
632 numbers compared to controls. We suggest that the difference between our findings and those of
633 Lobell *et al*. (2017) might be attributable to differences in genetic backgrounds. Nevertheless, the wild-
634 type number of ovarioles established in our *bin3* mutants is not sufficient to promote a normal egg-
635 laying rate. Egg-laying is in part a neuromuscular process, as muscle contractions of the ovary and
636 uterus promote successful oviposition (i.e., egg-laying; Deady and Sun 2015; Irizarry and Stathopoulos
637 2015; Liao and Nässel 2020; Garrett *et al.* 2023). It is possible, therefore, that defects in neuromuscular

638 function that we observe in *bin3* mutants (see below) might also explain why *bin3* mutant females lay
639 fewer eggs, *e.g.*, due to a reduction in the frequency or strength of these contractions.
640
641 **Conserved role of Bin3 and MEPCE in metazoan neurodevelopment**
642 A patient with a neurodevelopmental disorder characterized by mobility and musculature
643 deficiencies was shown to carry a heterozygous nonsense mutation in *MEPCE* (Schneeberger *et al.*
644 2019). Similarly, we found that *bin3* mutant flies exhibited difficulties in climbing and an inability to
645 properly fold their wings, phenotypes that are characteristic of neuromuscular defects (Shukla *et al.*
646 2013; Kairamkonda and Nongthomba 2014; Sanhueza *et al.* 2014; Manjila and Hasan 2018). Many
647 mutations in *Drosophila* can affect wing posture (see below), including those in the highly-conserved
648 JAK/STAT pathway (Harrison *et al.* 1998; Callus and Mathey-Prevot 2002; Ayala-Camargo *et al.* 2013;
649 Hatini *et al.* 2013; Johnstone *et al.* 2013). Therefore, the conserved roles of Bin3 and MEPCE in
650 metazoan neurodevelopment may occur through the JAK/STAT pathway. While the exact mechanisms
651 remain to be determined, the phenotypes we observe in *bin3* mutants (egg-laying, climbing, wing
652 posture) can be attributable to neuromuscular defects, suggesting a strong conservation in the
653 developmental function of Bin3 and MePCE in *Drosophila* and human development.
654 Bin3/MEPCE methylates the gamma phosphate on the 5′ end of the 7SK snRNA, while another
655 class of RNA methyltransferases methylates the N^6 position of internal adenosines (N^6-
656 methyladenosine, m^6A) on "RRACH" motifs (Wang *et al.* 2018) in a variety of RNAs (Lence *et al.* 2018).
657 Interestingly, both human 7SK (Warda *et al.* 2017; Leger *et al.* 2021; Perez-Pepe *et al.* 2023) and mouse
658 7SK (Xu *et al.* 2022) contain the m^6A modification. In HeLa cells, methylation of 7SK by the METLL3
659 m^6A "writer" protein in response to EGF signaling allows hnRNPs to associate with 7SK; this causes
660 HEXIM to dissociate from the 7SK snRNP and release P-TEFb, which activates transcriptional
661 elongation (Perez-Pepe *et al.* 2023). In mice, methylation of 7SK at adenine 281 by METLL3 is required

662 for the binding of m^6A "reader" proteins to establish proper 7SK secondary structure (Xu *et al.* 2022).
663 *Drosophila* 7SK contains a single RRACH motif at position 397-401; however, it is not known whether
664 the adenine within this motif is methylated, or if m^6A at that position would serve functions similar to
665 those in HeLa cells or mice. Intriguingly, flies mutant for m^6A writers (and m^6A readers) exhibit the
666 same neuromuscular defects in both climbing and resting wing posture (Lence *et al.* 2016; Kan *et al.*
667 2017) as flies mutant for *bin3* (this study). Therefore, it is possible that *Drosophila* 7SK might also
668 contain the m^6A modification (at A399), and that m^6A is important for 7SK stability and function in
669 neurodevelopmental processes in *Drosophila*.
670 Although Bin3 and the m^6A pathway might function synergistically to promote 7SK stability and
671 function, they seem to act antagonistically on transcription elongation: Bin3 is required to *prevent*
672 RNAPII pause-release, whereas the m^6A pathway has been shown in *Drosophila* to *promote* RNAPII
673 pause-release (Akhtar *et al.* 2021). Clearly, there is a complex balance between 7SK stability (via Bin3
674 binding and possible m^6A methylation) as well as 7SK functions that sequester P-TEFb (Bin3-mediated
675 function) or release P-TEFb (m^6A modification function) that is governed by the activities of diverse
676 classes of RNA methyltransferases, which in *Drosophila* contribute to neuromuscular function.
677 Moreover, it appears that m6A modifications in 7SK might serve species-specific roles in 7SK biology.
678 Neuromuscular disorders arise from developmental defects in motoneurons and/or the muscles
679 that they control. We attempted to identify the cells and tissues that require Bin3 for neuromuscular
680 function by performing an RNAi screen using over 90 GAL4 drivers active in specific neuron and muscle
681 cell types that drive the expression of two different short hairpin RNAs (shRNAs) targeting *bin3* coding
682 sequence (Ni *et al.* 2011). However, we did not identify any conditions under which *bin3* RNAi
683 knockdown recapitulated the neuromuscular phenotypes of *bin3* mutant flies. The failure of our screen
684 might be due to technical reasons such as weak GAL4 drivers and/or insufficient levels of RNAi
685 knockdown, or they could be due to Bin3 being required in more than one tissue simultaneously for

686 neuromuscular activity. Indeed, knockdown of *bin3* induced by the Trojan-GAL4 *bin3* allele (which also
687 functions as a null allele) in the spatiotemporal expression pattern of *bin3* recapitulated the *held-out*
688 *wings* phenotype of *bin3* mutant flies (data not shown), suggesting that Bin3 might be required in
689 multiple cell types simultaneously, at least for normal resting wing posture.
690

691 **Bin3 catalytic activity is dispensable for 7SK stability and snRNP function *in vivo***

692 MEPCE modifies the 5′ end of 7SK RNA by catalyzing the addition of a monomethyl cap to the
693 gamma phosphate (Gupta *et al.* 1990b; Shumyatsky *et al.* 1990; Jeronimo *et al.* 2007; Xue *et al.* 2010;
694 Yang *et al.* 2019). It has long been thought that the monomethyl cap is essential for 7SK stability. For
695 example, *in vitro* transcribed capped 7SK was more stable than uncapped 7SK when injected into
696 *Xenopus* oocytes (Shumyatsky *et al.* 1993). However, whether 7SK requires a monomethyl cap for
697 stability *in vivo* has never been adequately addressed. We and others have shown that Bin3 and its
698 orthologs are essential for 7SK stability, as deletion of *bin3* (Singh *et al.* 2011), siRNA-mediated
699 knockdown of *MEPCE* in human cells (Jeronimo *et al.* 2007; Xue *et al.* 2010), and morpholino-mediated
700 disruption of *mepcea* splicing in zebrafish embryos (Barboric *et al.* 2009) reduces 7SK levels.
701 Importantly, these approaches do not explicitly test the *in vivo* requirement for methyltransferase
702 activity, which requires the use of catalytic mutants.

703 Catalytic mutants of MEPCE have been characterized *in vitro*. A triple mutation in the active site
704 (V447A, L448A, and D449A) abolished methyltransferase activity, likely by preventing the interaction
705 between MEPCE and the methyl donor *S*-adenosyl-□-methionine (SAM). However, this mutant is also
706 defective for binding to 7SK and therefore it is not a catalytic mutant *per se* (Xue *et al.* 2010). A double
707 mutant in the active site (G451A and G455A) also abolished MEPCE methyltransferase activity, again,
708 presumably by preventing the interaction between MEPCE and SAM; however, this mutant does bind
709 to 7SK (Shelton *et al.* 2018). Finally, a single amino acid mutation in the active site (Y421A) reduced

710 methyltransferase activity to 0.6% that of the wt enzyme. This is likely due to loss of hydrogen bonds
711 between Y421 and both an adjacent residue (R425) and the 7SK gamma phosphate, which is the
712 recipient of the methyl group from SAM (Yang *et al.* 2019). Importantly, Y421A is not expected to
713 disrupt binding to either the methyl donor co-factor or the RNA substrate, but rather to disrupt the
714 chemistry of methyl transfer to the gamma phosphate (Yang *et al.* 2022). Therefore, given the precise
715 and specific nature of this active site mutation, our preferred choice for *in vivo* study of the importance
716 of methyl capping was a Y795A substitution in Bin3 (orthologous to Y421A in MEPCE).

717 Unexpectedly, we found that the Bin3^{Y795A} mutant did not exhibit any of the physiological
718 defects exhibited by *bin3* deletion mutants, suggesting that catalytic activity is not required for Bin3
719 function *in vivo* (**Fig. 8a**). This result could be explained, in part, by our finding that Bin3^{Y795A} still bound
720 and stabilized 7SK no differently than Bin3^{wt}, despite its expected lack of methyltransferase activity
721 (**Fig. 7b**). Thus, flies expressing the Bin3^{Y795A} allele retain the ability to assemble the 7SK snRNP to
722 repress P-TEFb and promote normal development. Our findings suggest that *in vivo* capping of
723 endogenous 7SK is not required for its stability *per se*, so long as Bin3 is able to bind to 7SK.

724 That the Bin3^{Y795A} catalytic mutant protein was still able to bind to 7SK is not entirely surprising.
725 Y421 in MEPCE (analogous to Y795 in Bin3) is located within a disordered region that becomes ordered
726 upon binding to 7SK, forming an alpha helix (Yang *et al.* 2022); this disorder-to-order transition is
727 required for MEPCE methyltransferase activity. When LARP7 binds to 7SK and then associates with
728 MEPCE, the alpha helix containing Y421 becomes disordered again (Yang *et al.* 2022); this order-to-
729 disorder transition induced by LARP7 binding inhibits MEPCE methyltransferase activity (Xue *et al.*
730 2010; Brogie and Price 2017; Yang *et al.* 2022). Therefore, MEPCE bound by LARP7 effectively
731 phenocopies MEPCE with a Y421A mutation, which is catalytically-dead (Yang *et al.* 2019). Thus, it
732 appears that Y421 in MEPCE and Y795 in Bin3 are not essential for 7SK binding, but instead are
733 essential only for methyl capping.

734 Our finding that the Bin3^{Y795A} catalytic mutant protein not only bound 7SK, but stabilized 7SK
735 despite the expected lack of catalytic activity, suggests that RNA binding contributes more to 7SK
736 stability than does methyl capping, challenging the assumption that the gamma monomethyl cap is
737 essential for 7SK stability. This is underscored by the fact that U6 snRNA, which binds to and is
738 presumed to be capped by Bin3 and its orthologs, is stable in the absence of these proteins (Jeronimo *et*
739 *al.* 2007; Muniz *et al.* 2013; Páez-Moscoso *et al.* 2022; Porat *et al.* 2022).
740 Bin3 and its orthologs are peculiar enzymes, in that they remain associated with the products of
741 the reaction they catalyze (Xue *et al.* 2010; Yang *et al.* 2019, 2022). MEPCE has a higher affinity both for
742 capped 7SK and SAH (the products) than uncapped 7SK and SAM (the reactants) (Yang *et al.* 2019).
743 Therefore, the gamma monomethyl cap might be required not for 7SK stability *per se*, but to enhance
744 the binding of MEPCE to the 5′ end of 7SK to keep the enzyme bound after catalyzing the
745 methyltransferase reaction. Constitutive binding of MEPCE to 7SK would serve the dual purposes of
746 physically protecting 7SK from inorganic phosphatases (for which the gamma monomethyl cap is a
747 substrate; Shumyatsky *et al.* 1990), and aiding in the recruitment of LARP7, which binds weakly to 7SK
748 in the absence of MEPCE (Xue *et al.* 2010), but enhances the affinity of MEPCE for 7SK after binding
749 (Muniz *et al.* 2013; Yang *et al.* 2022). However, our finding that the Bin3^{Y795A} catalytic mutant bound as
750 much 7SK as Bin3^{wt} despite the lack of a gamma monomethyl cap is not consistent with such a model
751 (at least not *in vivo*). Instead, our results support a model in which 7SK RNA secondary structure—and
752 not the gamma monomethyl cap—is required for Bin3 and its orthologs to bind to 7SK. Indeed, MEPCE
753 bound equally well to transfected 7SK harboring either the normal gamma monomethyl cap or a tri-
754 methyl guanosine (TMG) cap (Muniz *et al.* 2013), and Bmc1 (the *S. pombe* ortholog of Bin3) binds to
755 both gamma monomethyl-capped U6 RNA and TMG-capped telomerase RNA (Páez-Moscoso *et al.*
756 2022; Porat *et al.* 2022). These findings suggest that a gamma monomethyl cap structure is not
757 specifically required for constitutive or high-affinity binding by MEPCE and its orthologs. Alternatively,

758 7SK secondary structure features likely mediate initial association with MEPCE (i.e., prior to the
759 association of LARP7, which enhances the affinity of MEPCE for 7SK). When MEPCE initially binds to
760 7SK in the "nascent" conformation (adopted during 7SK synthesis), there is extensive hydrogen
761 bonding between the methyltransferase domain and the 5′ hairpin of 7SK (Yang *et al.* 2019). Binding of
762 MEPCE to 7SK requires the first two (Singh *et al.* 1990) to three (Muniz *et al.* 2013) base pairs of the 5′
763 hairpin, and a portion of the single-stranded DNA 3′ to the hairpin (Shumyatsky *et al.* 1994; Muniz *et al.*
764 2013; Yang *et al.* 2019). Subsequently, LARP7 binds to the complex of MEPCE and 7SK, and the
765 conformation of 7SK changes from a "nascent" conformation to a "closed" conformation (adopted after
766 formation of the core snRNP of MEPCE, 7SK, and LARP7). In this conformation, MEPCE forms
767 additional hydrogen bonds to 7SK, and thereby has higher affinity for the "closed" conformation of 7SK
768 than for the "nascent" conformation of 7SK (Yang *et al.* 2022). Therefore, both 7SK secondary structure
769 and association with LARP7 are likely the major contributors to the constitutive binding of MEPCE to
770 7SK.

771 One possible circumstance under which the gamma monomethyl cap on 7SK might be essential
772 for stability is when the 7SK snRNP is actively repressing P-TEFb. For HEXIM to bind to 7SK and
773 sequester P-TEFb, 7SK must undergo a conformational change from the "closed" conformation (i.e.,
774 the "core" snRNP conformation) to the "linear" conformation (i.e., the "repressive" snRNP
775 conformation). In this conformation, the 5′ end of 7SK is located outside of the MEPCE active site
776 (Yang *et al.* 2022), and therefore, in the context of the repressive 7SK snRNP, the 5′ end of 7SK might
777 be solvent-exposed, which would necessitate a gamma monomethyl cap to protect 7SK from
778 exoribonucleolytic degradation. However, these findings are based on crystal structures using a
779 recombinant MEPCE comprising only the methyltransferase domain. Our finding that 7SK is not only
780 bound but is also stabilized by $Bin3^{Y795A}$ catalytic mutant protein (just like $Bin3^{wt}$ protein) leaves open
781 the possibility that there are regions outside of the methyltransferase domain in full-length

782 Bin3/MEPCE that protects the 5′ end of 7SK, even when located outside of the active site. Moreover,
783 the finding that the 5′ end of 7SK might not be bound by MEPCE when in the "linear" conformation
784 further supports a model in which the gamma monomethyl cap is not required for constitutive binding
785 of MEPCE to 7SK.

786 If the monomethyl cap is not required for either 7SK stability or for Bin3 binding, then what is
787 the purpose of the methyltransferase domain in Bin3 and its orthologs? One possibility is that the
788 methyltransferase domain is a vestige of an ancestral ortholog of Bin3 that did not remain
789 constitutively bound to its RNA substrates, and therefore, the monomethyl cap would have been
790 essential to protect these RNAs from 5′-3′ exoribonucleolytic degradation. The acquisition of
791 additional protein binding constituents during evolution of a primordial 7SK snRNP complex might have
792 necessitated that Bin3 remain associated with 7SK (after catalyzing the methyltransferase reaction) to
793 facilitate the stable interaction of these additional components (like Larp7). This process would have
794 rendered the monomethyl capping reaction dispensable for 7SK stability, as we observe. A second
795 possibility, supported by the strong conservation of the methyltransferase domain over evolutionary
796 time, argues that catalytic activity has an important function that has yet to be identified, perhaps on
797 substrates other than 7SK.

798

799 **A metazoan-specific motif in Bin3 facilitates a 7SK-independent, tissue-specific function in**
800 **neurodevelopment**

801 *S. pombe* Bmc1, the most ancient ortholog of Bin3 studied to date, consists only of the
802 conserved methyltransferase domain (Cosgrove *et al.* 2012; Páez-Moscoso *et al.* 2022; Porat *et al.*
803 2022). Over the course of evolution, Bin3 orthologs gained additional protein sequence flanking the
804 methyltransferase domain (Cosgrove *et al.* 2012). We found a 16-amino acid motif N-terminal to the
805 methyltransferase domain that is highly conserved in metazoans, and is mostly unstructured. Given its

806 location outside of the methyltransferase domain, we were not surprised to find that this metazoan-
807 specific motif (MSM) was not required for Bin3 to bind or stabilize 7SK *in vivo*, and consequently, was
808 dispensable for fecundity and climbing ability. What we did not expect, however, was that flies
809 expressing Bin3 deleted of the MSM (Bin3$^{\Delta MSM}$) were unable to properly fold their wings, phenocopying
810 *bin3* null mutants (**Fig. 7c**). These findings suggest that the Bin3 MSM plays a tissue-specific role in gene
811 regulation independent of 7SK (**Fig. 8b**). There is likely one or more MSM-interacting proteins that help
812 Bin3 regulate gene expression. These proteins might be specifically expressed in the tissues involved in
813 wing posture (*e.g.*, the direct and indirect flight muscles), or they might be ubiquitously expressed, but
814 the interaction with the Bin3 MSM is essential for Bin3 function only in tissues contributing to normal
815 resting wing posture. Moreover, this protein might be incorporated into the core snRNP of 7SK, Bin3,
816 and Larp7 to generate a novel 7SK snRNP, or the association with Bin3 MSM might be independent of
817 the 7SK snRNP altogether.
818 A 7SK-independent function of Bin3 is not without precedent. It was previously shown that
819 fibroblasts from a patient with a nonsense mutation in *MEPCE* (*MEPCE* haploinsufficient cells) and cells
820 deleted of *LARP7* (*LARP7* KO cells) both had reduced levels of 7SK, as expected, but that genes up-
821 regulated in *MEPCE* haploinsufficient cells were not affected in *LARP7* KO cells. Moreover, exogenous
822 *MEPCE* rescued the up-regulation phenotype of *MEPCE* haploinsufficient cells, despite only leading to a
823 small increase in 7SK levels. Based on these findings, Schneeberger *et al*. (2019) hypothesized that
824 MEPCE might have a 7SK-independent role in regulating transcription, potentially by interacting with
825 as-yet unknown proteins. Our finding that Bin3$^{\Delta MSM}$ binds and stabilizes 7SK but is not sufficient to
826 rescue all *bin3* mutant phenotypes supports this hypothesis and suggests that the as-yet unknown
827 proteins that interact with Bin3/MEPCE to regulate transcription does so through the MSM,
828 independent of the 7SK snRNP.
829

830 **Conclusions**

831 In summary, we have carried out the first detailed *in vivo* study of the highly-conserved
832 Bin3/MEPCE RNA methyltransferase in a metazoan host. The surprising results demonstrate the value
833 of rigorously testing models for enzyme function in whole organisms. Our study establishes *Drosophila*
834 as a genetically tractable developmental model for further dissection of Bin3/MEPCE and 7SK non-
835 coding RNA pathways, and how their disruption may be associated with human disease.

836 **DATA AVAILABILITY**

837 Plasmids and *Drosophila* stocks are available upon request. All reagent inquiries should be directed to
838 RJP. All data required to confirm the conclusions made in this article are presented in the text, figures,
839 and tables.

840

841 **ACKNOWLEDGEMENTS**

842 We are grateful to the Bloomington *Drosophila* Stock Center (NIH Grant P40OD018537) for fly stocks,
843 the *Drosophila* Genomics Resource Center (NIH Grant 2P40OD010949) for plasmid pUASP-attB; Jian-
844 Quan Ni for plasmid pNP; BestGene, Inc. for generating transgenic flies; and David Price for anti-CycT
845 antiserum. We are also grateful to Scott Neal, Mark Bayfield, and Jennifer Porat for helpful discussions.

846

847 **FUNDING**

848 This work and RJP was supported by grants to S. Hanes (NSF MCB-1515076 and NIH R-01 GM123985-
849 01) and B. Knutson (NIGMS R01-GM141033).

850

851 **CONFLICTS OF INTEREST**

852 None declared.

853 **FIGURE LEGENDS**

854 **Figure 1. Molecular characterization of *bin3* mutant and rescue flies. (a)** Graphic depicting the ~26 kb
855 *bin3* locus on chromosome 2R (cytogenetic bands 42A13-42A14). Two promoters, P1 and P2 (grey),
856 drive expression of *bin3* (Zhu and Hanes 2000; Singh *et al.* 2011). The *bin3* ORF (salmon) comprises 6
857 coding exons. $bin3^{\Delta}$ refers to the $bin3^{2\text{-}7}$ excision allele created by FLP/FRT-mediated recombination
858 between transposon insertions *PBac{RB}*$bin3^{e02231}$ and *P{XP}d02161* (Parks *et al.* 2004; Singh *et al.* 2011).
859 *Df* refers to deficiency *Df(2R)ED1612*, which deletes ~829 kb of chromosome 2R, including promoter P1
860 and all *bin3* coding sequence (Ryder *et al.* 2004). $bin3^{\Delta}$ and *Df* in *trans* produce *bin3* mutant flies. $bin3^{+}$
861 (sky blue) is a transgenic insertion of a BAC comprising ~20 kb of chromosome 2R, including promoter
862 P1 and all *bin3* coding sequence. In $bin3^{2\text{-}7}$*/Df* flies, this insertion rescues *bin3* mutant phenotypes. **(b-d)**
863 Bar graphs showing the average amount of *bin3* mRNA (b), 7SK snRNA (c), and U6 snRNA (d) in total
864 RNA extracted from ovaries of females of the indicated genotypes, for three biological replicates. Note
865 that *bin3* mRNA was below the level of detection in $bin3^{2\text{-}7}$*/Df* and $bin3^{2\text{-}7}$*/Df;* $CycT^{j11B2}$/+ ovaries for 2 of
866 the three biological replicates. RNA levels were normalized to *rp49* mRNA and made relative to wt
867 using CFX Maestro 2.0 (version 5.2.008.0222, Bio-Rad). Error bars represent the standard error of the
868 mean. Statistical significance was calculated by unpaired t-test using CFX Maestro 2.0 (version
869 5.2.008.0222, Bio-Rad). *P* values of <.05 (*), <0.001 (***), <.0001 (****), and not significant (ns) are
870 indicated. **(e)** Western blot for CycT (Nguyen *et al.* 2012) and Actin in extracts prepared from ovaries of
871 females of the indicated genotypes. The *P{lacW}j11B2*^{j11B2} insertion (Spradling *et al.* 1999) into one of the
872 two different *CycT* 5' -UTRs reduces expression of the large isoform of CycT.

873

874 **Figure 2. Bin3 is ubiquitously expressed in the ovary and is required for egg-laying, but is not**
875 **required to establish ovarioles and does not function in germline to promote egg-laying. (a)** Scatter
876 plot showing the egg-laying rates of females of the indicated genotypes for each of three biological

877 replicates. Error bars represent the standard deviation. Statistical significance compared to *bin3*$^{2-7}$*/Df*
878 was calculated by nested one-way ANOVA with Dunnett's Correction for multiple comparisons, using
879 Prism (version 9.4.1, GraphPad). *P* values of <.001 (***) and <.0001 (****) are indicated. **(b)** Cartoon
880 depicting a single ovariole, of which 16-20 make up a single adult ovary. Germline cells are indicated in
881 pink, nurse cell nuclei (arrow) are indicated in purple, oocytes are indicated in blue, and somatic cells
882 surrounding the germline and oocytes are indicated in purple. **(c to d')** Immunofluorescence staining of
883 adult ovaries for 3xHA-Bin3 (green), Vasa (a cytoplasmic marker for germline cells; blue), and Hoechst
884 staining of DNA (red). Scale bars = 100 µm. A Trojan-GAL4 phase 0 insertion in *bin3* (*bin3*$^{TG4.0}$) was used
885 to drive expression of a *UAS-3xHA-bin3* transgene in the pattern of *bin3* expression (*bin3*$^{TG4.0}$ > *UAS-bin3-*
886 *3xHA*). 3xHA-Bin3 localizes to the nuclei of all germline and somatic cells (C-C'). No HA staining was
887 detected in *bin3*$^{TG4.0}$ control ovaries (D-D'), demonstrating the specificity of HA staining in *bin3*$^{TG4.0}$ >
888 *UAS-3xHA-bin3* ovaries. **(e-f')** Single-molecule fluorescence *in situ* hybridization (smFISH) of adult
889 ovaries for 7SK (green) and Hoechst staining of DNA (purple). Scale bars = 100 µm. 7SK localizes to the
890 nuclei of all germline and somatic cells in wt ovaries (E-E'). 7SK staining is absent in *bin3*$^{2-7}$*/Df* ovaries
891 (F-F'), which do not accumulate 7SK (see Fig. 1c). **(g)** Scatter plot showing the mean number of
892 ovarioles per ovary per female of the indicated genotypes for each of two biological replicates. Error
893 bars represent the standard deviation. Statistical significance compared to *bin3*$^{2-7}$*/Df* was calculated by
894 nested one-way ANOVA with Dunnett's Correction for multiple comparisons, using Prism (version
895 9.4.1, GraphPad). *P* values of not significant (ns) are indicated. **(h)** Scatter plot showing the absolute
896 value of the difference between ovariole number within a pair of ovaries per female of the indicated
897 genotypes for each of two biological replicates. Error bars represent the standard deviation. Statistical
898 significance compared to *bin3*$^{2-7}$*/Df* was calculated by nested one-way ANOVA with Dunnett's
899 Correction for multiple comparisons, using Prism (version 9.4.1, GraphPad). *P* values of not significant
900 (ns) are indicated. **(i)** Scatter plot showing the egg-laying rates of females of the indicated genotypes

901 for each of three biological replicates. Error bars represent the standard deviation. Statistical
902 significance compared to *bin3*$^{2\text{-}7}$*/Df; nanos-GAL4::VP16/+* was calculated by nested one-way ANOVA
903 with Dunnett's Correction for multiple comparisons, using Prism (version 9.4.1, GraphPad). *P* values of
904 <.05 (*), <.001 (***) and not significant (ns) are indicated.
905
906 **Figure 3. Bin3 is required for neuromuscular function. (a)** Scatter plot showing the percent of flies of
907 the indicated genotypes climbing 8 cm in 12" in each of 10 trials, for each of three biological replicates.
908 Error bars represent the standard deviation. Statistical significance compared to *bin3*$^{2\text{-}7}$*/Df* was
909 calculated by nested one-way ANOVA with Dunnett's Correction for multiple comparisons, using Prism
910 (version 9.4.1, GraphPad). *P* value of <.001 (***) is indicated. **(b-e)** Images of females of the indicated
911 genotypes, exhibiting either a normal resting wing posture or a *held-out wings* phenotype. **(f)** Scatter
912 plot showing the percent of flies of the indicated genotypes climbing 8 cm in 12" in each of 4 trials, for
913 each of three biological replicates. Error bars represent the standard deviation. Statistical significance
914 was calculated by nested t-test, using Prism (version 9.4.1, GraphPad). *P* value of not significant (ns) is
915 indicated. **(g-h)** Images of females of the indicated genotypes, exhibiting either a normal resting wing
916 posture or a *held-out wings* phenotype.
917
918 **Figure 4. Molecular characterization of the *bin3*$^{TG4.0}$ Trojan GAL4 allele and Bin3 protein mutants.**
919 **(a)** Bin3 modeled onto the crystal structure of 309 amino acids of the MEPCE active site (Yang *et al.*
920 2019). Y421 in MEPCE (black) is juxtaposed between the 7SK 5' gamma phosphate (orange and
921 salmon) and *S*-adenosyl-*L*-homocysteine (SAH, blue and gold), and is essential for MEPCE catalytic
922 activity *in vitro* (Yang *et al.* 2019). Y795 in Bin3 (red) aligns with Y421 in MEPCE (RMSD = 0.000). **(b)**
923 Same as in (a), but with the Y421A (MEPCE, black) and Y795A (Bin3, red) tyrosine-to-alanine mutations
924 introduced. Y421A completely eliminated MEPCE catalytic activity *in vitro* (Yang *et al.* 2019). **(c)** Partial

925 alignment of Bin3 orthologs from *D. melanogaster*, *H. sapiens* (MEPCE), *D. rerio* (BCDIN3), and *S. pombe*
926 (Bmc1). Conserved residues are in boldface. **(d)** Graphic depicting the *bin3* locus, as in **Fig. 1a**. *bin3*$^{TG4.0}$
927 refers to a transgenic insertion of a Trojan GAL4 phase 0 (TG4.0) construct into the second intron in the
928 *bin3* ORF (Lee *et al.* 2018). A splice acceptor (SA) in the insertion causes the TG4.0 cassette to be spliced
929 into the *bin3* mRNA; transcription is terminated at the end of the cassette by a synthetic poly(A)
930 sequence. When the chimeric *bin3*$^{TG4.0}$ mRNA is translated, T2A, a viral peptide sequence, disrupts
931 translation and causes the release of the nonfunctional Bin3:T2A chimeric peptide from the ribosome;
932 subsequently, the ribosome resumes translation of full-length GAL4 protein. *Df* refers to deficiency
933 *Df(2R)BSC313*, which deletes ~625 kb of chromosome 2R, including promoters P2 and P1, and all *bin3*
934 coding sequence (Cook *et al.* 2012). *bin3*$^{TG4.0}$ and *Df* in *trans* produce *bin3* mutant flies that express *GAL4*
935 in the pattern of *bin3* expression. GAL4 then binds to UAS and drives expression of *UAS-bin3* transgenes
936 (see **Fig. 4h-j**). **(e-g)** Bar graphs showing the average amount of *bin3* mRNA (e), 7SK snRNA (f), and U6
937 snRNA (g) in total RNA extracted from ovaries of females of the indicated genotypes, for three
938 biological replicates. RNA levels were normalized to *rp49* mRNA and made relative to wt using CFX
939 Maestro 2.0 (version 5.2.008.0222, Bio-Rad). Error bars represent the standard error of the mean.
940 Statistical significance was calculated by unpaired t-test using CFX Maestro 2.0 (version 5.2.008.0222,
941 Bio-Rad). *P* values of <.05 (*), <0.01 (**), <.0001 (****), and not significant (ns) are indicated. **(h-j)**
942 Graphic depicting *UAS-DSCP-3xHA-bin3* transgenes. UAS-DSCP (grey) is a GAL4-responsive promoter
943 that is active in both germline and somatic cells (Pfeiffer *et al.* 2008). *bin3* cDNAs encode Bin3 proteins
944 that are either wt (h; sky blue), catalytically-dead (I; Y795A, pink), or deleted of the MSM (j; ΔMSM,
945 maroon). Each construct is tagged at the C-terminus with 3xHA that is codon-optimized for *Drosophila*
946 (green). When these transgenes are independently crossed into the *bin3*$^{TG4.0}$*/Df* background (see **Fig.**
947 **4d**), flies will express only 3xHA-Bin3, 3xHA-Bin3^{Y795A}, or 3xHA-Bin3$^{\Delta MSM}$ proteins, respectively. **(k)** Bar
948 graph showing the average amount of *bin3* mRNA in total RNA extracted from ovaries of females of the

949 indicated genotypes, for three biological replicates. RNA levels were normalized to *rp49* mRNA and
950 made relative to *bin3*$^{TG4.0}$*/Df; UAS-bin3/+* using CFX Maestro 2.0 (version 5.2.008.0222, Bio-Rad). Error
951 bars represent the standard error of the mean. Statistical significance was calculated by unpaired t-test
952 using CFX Maestro 2.0 software (version 5.2.008.0222, Bio-Rad). *P* value of not significant (ns) is
953 indicated. All three *UAS-bin3* transgenes are expressed to similar levels. **(i)** Representative Western blot
954 for 3xHA-Bin3 proteins and Actin in extracts prepared from ovaries of females of the indicated
955 genotypes. The relative amounts of 3xHA-Bin3^{Y795A} and 3xHA-Bin3$^{\Delta MSM}$ relative to 3xHA-Bin3 (wt) ± the
956 standard deviation from two biological replicates are indicated below. Statistical significance was
957 calculated by ordinary one-way ANOVA with Dunnett's Correction for multiple comparisons with a
958 single pooled variance, using Prism (version 9.4.1, GraphPad). *P* values of <0.05 (*) and not significant
959 (ns) are indicated. All three transgenes produce similar amounts of 3xHA-Bin3 proteins.
960
961 **Figure 5. Neither catalytic activity nor the metazoan-specific motif are required for 7SK or U6**
962 **binding and stability. (a** and **c)** Bar graphs showing the average amount of 7SK (a) and U6 (c) RNAs in
963 total RNA extracted from ovaries of females of the indicated genotypes, for three biological replicates.
964 RNA levels were normalized to *rp49* mRNA and made relative to *bin3*$^{TG4.0}$*/Df; UAS-bin3/+* using CFX
965 Maestro 2.0 (version 5.2.008.0222, Bio-Rad). Error bars represent the standard error of the mean.
966 Statistical significance was calculated by unpaired t-test using CFX Maestro 2.0 (version 5.2.008.0222,
967 Bio-Rad). *P* value of not significant (ns) is indicated. **(b** and **d)** Bar graphs showing the average amount
968 of 7SK (b) and U6 (d) RNA bound by 3xHA-Bin3 proteins immunoprecipitated with anti-HA magnetic
969 beads from extracts prepared from ovaries of females of the indicated genotypes, for three biological
970 replicates. The ratio of immunoprecipitated RNA to input RNA, from flies expressing 3xHA-Bin3
971 proteins relative to flies not expressing 3xHA-Bin3 proteins (*bin3*$^{TG4.0}$/+), was calculated using CFX
972 Maestro 2.0 (version 5.2.008.0222, Bio-Rad). Error bars represent the standard error of the mean.

973 Statistical significance compared to *bin3*$^{TG4.0}$/+ (black asterisks) or *bin3*$^{TG4.0}$*/Df; UAS-bin3*/+ (sky blue
974 asterisks) was calculated by one-way ANOVA with Benjamini-Hochberg correction for false discovery
975 rate, using CFX Maestro 2.0 (version 5.2.008.0222, Bio-Rad). *P* values of <0.05 (*), <.01 (**), <.0001
976 (****), and not significant (ns) are indicated.
977
978 **Figure 6. Phenotypic characterization of Bin3^{Y795A} and Bin3$^{\Delta MSM}$ mutant proteins *in vivo*. (a)** Scatter
979 plot showing egg-laying rates of females of the indicated genotypes for each of three biological
980 replicates. Error bars represent the standard deviation. Statistical significance compared to *bin3*$^{TG4.0}$*/Df*
981 (salmon asterisks) or *bin3*$^{TG4.0}$*/Df; UAS-bin3*/+ (sky blue asterisks) was calculated by nested one-way
982 ANOVA with Dunnett's Correction for multiple comparisons, using Prism (version 9.4.1, GraphPad). *P*
983 values of <.01 (**), <0.001 (***), <.0001 (****), and not significant (ns) are indicated. **(b)** Scatter plot
984 showing the percent of flies of the indicated genotypes climbing 8 cm in 12" in each of 10 trials, for each
985 of three biological replicates. Error bars represent the standard deviation. Statistical significance
986 compared to *bin3*$^{TG4.0}$*/Df* (salmon asterisks) or *bin3*$^{TG4.0}$*/Df; UAS-bin3*/+ (sky blue asterisks) was calculated
987 by nested one-way ANOVA with Dunnett's Correction for multiple comparisons, using Prism (version
988 9.4.1, GraphPad). *P* values of <.0001 (****) and not significant (ns) are indicated. **(c-h)** Images of
989 females of the indicated genotypes, exhibiting either a normal resting wing posture or a *held-out wings*
990 phenotype.
991
992 **Figure 7. Summary of Bin3^{wt}, Bin3^{Y795A}, and Bin3$^{\Delta MSM}$ protein functions. (a)** Bin3^{wt} binds, caps, and
993 stabilizes 7SK, which allows for P-TEFb to be sequestered and repressed, which prevents RNAPII pause-
994 release and promotes egg-laying, climbing, and normal resting wing posture. **(b)** Bin3^{Y795A} is able to
995 bind and stabilize 7SK despite being catalytically-dead; consequently, Bin3^{Y795A} also promotes egg-
996 laying, climbing, and normal resting wing posture. **(c)** Bin3$^{\Delta MSM}$ binds, caps, and stabilizes 7SK, and

997 represses P-TEFb; this is sufficient to promote normal egg-laying and climbing, but is not sufficient to
998 promote normal wing posture. This suggests the MSM confers a 7SK-independent, tissue-specific
999 function to Bin3.
1000
1001 **Figure 8. Model for the role of Bin3 in *Drosophila* development. (a)** Bin3 binds, caps, and stabilizes
1002 7SK; however, methyltransferase activity is not required for 7SK stability *in vivo*. Stabilized 7SK
1003 assembles a snRNP that represses P-TEFb, which prevents RNAPII transcription elongation. **(b)** The
1004 Bin3 MSM confers a 7SK-independent, tissue-specific function to Bin3. The MSM might mediate an
1005 interaction with a tissue-specific factor, or this interaction might only be important in specific tissues.
1006 Bin3 and this factor then repress transcription elongation by a mechanism that is likely downstream of
1007 P-TEFb.

1008 **SUPPLEMENTAL TABLES**

1009 **Table S1. Public fly stocks used in this study.** This table lists the publicly available fly stocks used in
1010 this study, including their genotypes as they appear in the paper, their detailed genotypes, the stock
1011 center from which they were procured, and the stock number.

1012

1013 **Table S2. Fly stocks produced for this study.** This table lists the fly stocks produced for this study,
1014 including their genotypes as they appear in the paper, their detailed genotypes, and a detailed
1015 description of how each fly stock was produced.

1016

1017 **Table S3. Flies used for experiments.** This table lists the flies used in each figure, including their
1018 genotypes as they appear in the paper, their detailed genotypes, the genotypes of the female and male
1019 flies crossed to produce flies used for experiments, and the figure(s) in which each fly is used.

1020 **REFERENCES**

1021 Abbaszadeh E. K., and E. R. Gavis, 2016 Fixed and live visualization of RNAs in Drosophila oocytes and
1022 embryos. Methods 98: 34–41. https://doi.org/10.1016/j.ymeth.2016.01.018

1023 Abuhashem A., V. Garg, and A.-K. Hadjantonakis, 2022 RNA polymerase II pausing in development:
1024 orchestrating transcription. Open Biol 12: 210220. https://doi.org/10.1098/rsob.210220

1025 Adelman K., and J. T. Lis, 2012 Promoter-proximal pausing of RNA polymerase II: emerging roles in
1026 metazoans. Nat Rev Genet 13: 720–731. https://doi.org/10.1038/nrg3293

1027 Akhtar J., Y. Renaud, S. Albrecht, Y. Ghavi-Helm, J.-Y. Roignant, *et al.*, 2021 m6A RNA methylation
1028 regulates promoter- proximal pausing of RNA polymerase II. Mol Cell 81: 3356-3367.e6.
1029 https://doi.org/10.1016/j.molcel.2021.06.023

1030 Ayala-Camargo A., A. M. Anderson, M. Amoyel, A. B. Rodrigues, M. S. Flaherty, *et al.*, 2013 JAK/STAT
1031 signaling is required for hinge growth and patterning in the Drosophila wing disc. Dev Biol 382: 413--
1032 426. https://doi.org/10.1016/j.ydbio.2013.08.016

1033 Baehrecke E. H., 1997 who encodes a KH RNA binding protein that functions in muscle development.
1034 Dev Camb Engl 124: 1323–32.

1035 Barboric M., T. Lenasi, H. Chen, E. B. Johansen, S. Guo, *et al.*, 2009 7SK snRNP/P-TEFb couples
1036 transcription elongation with alternative splicing and is essential for vertebrate development. Proc
1037 National Acad Sci 106: 7798–7803. https://doi.org/10.1073/pnas.0903188106

1038 Barrandon C., F. Bonnet, V. T. Nguyen, V. Labas, and O. Bensaude, 2007 The Transcription-Dependent
1039 Dissociation of P-TEFb-HEXIM1-7SK RNA Relies upon Formation of hnRNP-7SK RNA Complexes.
1040 Mol Cell Biol 27: 6996–7006. https://doi.org/10.1128/mcb.00975-07

1041 Blazek D., M. Barboric, J. Kohoutek, I. Oven, and B. M. Peterlin, 2005 Oligomerization of HEXIM1 via
1042 7SK snRNA and coiled-coil region directs the inhibition of P-TEFb. Nucleic Acids Res 33: 7000–7010.
1043 https://doi.org/10.1093/nar/gki997

1044 Brand A. H., and N. Perrimon, 1993 Targeted gene expression as a means of altering cell fates and
1045 generating dominant phenotypes. Development 118: 401–415.
1046 https://doi.org/10.1242/dev.118.2.401

1047 Brogie J. E., and D. H. Price, 2017 Reconstitution of a functional 7SK snRNP. Nucleic Acids Res 45: 6864–
1048 6880. https://doi.org/10.1093/nar/gkx262

1049 Brookes E., and A. Pombo, 2009 Modifications of RNA polymerase II are pivotal in regulating gene
1050 expression states. Embo Rep 10: 1213–1219. https://doi.org/10.1038/embor.2009.221

1051 Bugai A., A. J. C. Quaresma, C. C. Friedel, T. Lenasi, R. Düster, *et al.*, 2019 P-TEFb Activation by RBM7
1052 Shapes a Pro-survival Transcriptional Response to Genotoxic Stress. Mol Cell 74: 254-267.e10.
1053 https://doi.org/10.1016/j.molcel.2019.01.033

1054 Cabrera G. R., D. Godt, P. Fang, J. Couderc, and F. A. Laski, 2002 Expression pattern of Gal4 enhancer
1055 trap insertions into the bric à brac locus generated by P element replacement. Genesis 34: 62–65.
1056 https://doi.org/10.1002/gene.10115

1057 Callus B. A., and B. Mathey-Prevot, 2002 SOCS36E, a novel Drosophila SOCS protein, suppresses
1058 JAK/STAT and EGF-R signalling in the imaginal wing disc. Oncogene 21: 4812--4821.
1059 https://doi.org/10.1038/sj.onc.1205618

1060 Chan S.-K., and G. Struhl, 1997 Sequence-specific RNA binding by Bicoid. Nature 388: 634–634.
1061 https://doi.org/10.1038/41692

1062 Chen F. X., E. R. Smith, and A. Shilatifard, 2018 Born to run: control of transcription elongation by RNA
1063 polymerase II. Nat Rev Mol Cell Bio 19: 464–478. https://doi.org/10.1038/s41580-018-0010-5

1064 Cheng B., and D. H. Price, 2007 Properties of RNA Polymerase II Elongation Complexes Before and
1065 After the P-TEFb-mediated Transition into Productive Elongation*. J Biol Chem 282: 21901–21912.
1066 https://doi.org/10.1074/jbc.m702936200

1067 Chiba K., J. Yamamoto, Y. Yamaguchi, and H. Handa, 2010 Promoter-proximal pausing and its release:
1068 Molecular mechanisms and physiological functions. Exp Cell Res 316: 2723–2730.
1069 https://doi.org/10.1016/j.yexcr.2010.05.036

1070 Cho P. F., F. Poulin, Y. A. Cho-Park, I. B. Cho-Park, J. D. Chicoine, *et al.*, 2005 A New Paradigm for
1071 Translational Control: Inhibition via 5′-3′ mRNA Tethering by Bicoid and the eIF4E Cognate 4EHP.
1072 Cell 121: 411–423. https://doi.org/10.1016/j.cell.2005.02.024

1073 Cook R. K., S. J. Christensen, J. A. Deal, R. A. Coburn, M. E. Deal, *et al.*, 2012 The generation of
1074 chromosomal deletions to provide extensive coverage and subdivision of the Drosophila
1075 melanogaster genome. Genome Biol 13: R21. https://doi.org/10.1186/gb-2012-13-3-r21

1076 Core L., and K. Adelman, 2019 Promoter-proximal pausing of RNA polymerase II: a nexus of gene
1077 regulation. Gene Dev 33: 960–982. https://doi.org/10.1101/gad.325142.119

1078 Cosgrove M. S., Y. Ding, W. A. Rennie, M. J. Lane, and S. D. Hanes, 2012 The Bin3 RNA
1079 methyltransferase targets 7SK RNA to control transcription and translation. Wiley Interdiscip Rev
1080 Rna 3: 633–647. https://doi.org/10.1002/wrna.1123

1081 Deady L. D., and J. Sun, 2015 A Follicle Rupture Assay Reveals an Essential Role for Follicular
1082 Adrenergic Signaling in Drosophila Ovulation. Plos Genet 11: e1005604.
1083 https://doi.org/10.1371/journal.pgen.1005604

1084 Diao F., and B. H. White, 2012 A Novel Approach for Directing Transgene Expression in Drosophila:
1085 T2A-Gal4 In-Frame Fusion. Genetics 190: 1139–1144. https://doi.org/10.1534/genetics.111.136291

1086 Diao F., H. Ironfield, H. Luan, F. Diao, W. C. Shropshire, *et al.*, 2015 Plug-and-Play Genetic Access to
1087 Drosophila Cell Types using Exchangeable Exon Cassettes. Cell Reports 10: 1410–1421.
1088 https://doi.org/10.1016/j.celrep.2015.01.059

1089 Dollinger R., and D. S. Gilmour, 2021 Regulation of Promoter Proximal Pausing of RNA Polymerase II in
1090 Metazoans. J Mol Biol 433: 166897. https://doi.org/10.1016/j.jmb.2021.166897

1091 Doren M. V., A. L. Williamson, and R. Lehmann, 1998 Regulation of zygotic gene expression in
1092 Drosophila primordial germ cells. Curr Biol 8: 243–246. https://doi.org/10.1016/s0960-
1093 9822(98)70091-0

1094 Dubnau J., and G. Struhl, 1996 RNA recognition and translational regulation by a homeodomain
1095 protein. Nature 379: 694–699. https://doi.org/10.1038/379694a0

1096 Erdős G., and Z. Dosztányi, 2020 Analyzing Protein Disorder with IUPred2A. Curr Protoc Bioinform 70:
1097 e99. https://doi.org/10.1002/cpbi.99

1098 Erdős G., M. Pajkos, and Z. Dosztányi, 2021 IUPred3: prediction of protein disorder enhanced with
1099 unambiguous experimental annotation and visualization of evolutionary conservation. Nucleic Acids
1100 Res 49: gkab408-. https://doi.org/10.1093/nar/gkab408

1101 Fujinaga K., F. Huang, and B. M. Peterlin, 2023 P-TEFb: The master regulator of transcription
1102 elongation. Mol Cell 83: 393–403. https://doi.org/10.1016/j.molcel.2022.12.006

1103 Gabler F., S. Nam, S. Till, M. Mirdita, M. Steinegger, *et al.*, 2020 Protein Sequence Analysis Using the
1104 MPI Bioinformatics Toolkit. Curr Protoc Bioinform 72: e108. https://doi.org/10.1002/cpbi.108

1105 Gaertner B., and J. Zeitlinger, 2014 RNA polymerase II pausing during development. Development 141:
1106 1179–1183. https://doi.org/10.1242/dev.088492

1107 Garrett E. C., A. M. Bielawski, E. Ruchti, L. M. Sherer, I. Waghmare, *et al.*, 2023 The matricellular protein
1108 Drosophila CCN is required for synaptic transmission and female fertility. Genetics.
1109 https://doi.org/10.1093/genetics/iyac190

1110 Gilmour D. S., 2009 Promoter proximal pausing on genes in metazoans. Chromosoma 118: 1–10.
1111 https://doi.org/10.1007/s00412-008-0182-4

1112 Gonzalez M. N., D. Blears, and J. Q. Svejstrup, 2021 Causes and consequences of RNA polymerase II
1113 stalling during transcript elongation. Nat Rev Mol Cell Bio 22: 3–21. https://doi.org/10.1038/s41580-
1114 020-00308-8

1115 Gupta S., R. K. Busch, R. Singh, and R. Reddy, 1990a Characterization of U6 small nuclear RNA cap-
1116 specific antibodies. Identification of gamma-monomethyl-GTP cap structure in 7SK and several
1117 other human small RNAs. J Biol Chem 265: 19137–19142. https://doi.org/10.1016/s0021-
1118 9258(17)30635-x

1119 Gupta S., R. K. Busch, R. Singh, and R. Reddy, 1990b Characterization of U6 small nuclear RNA cap-
1120 specific antibodies. Identification of gamma-monomethyl-GTP cap structure in 7SK and several
1121 other human small RNAs. J Biological Chem 265: 19137–42.

1122 Haaland R. E., C. H. Herrmann, and A. P. Rice, 2005 siRNA depletion of 7SK snRNA induces apoptosis
1123 but does not affect expression of the HIV-1 LTR or P-TEFb-dependent cellular genes. J Cell Physiol
1124 205: 463–470. https://doi.org/10.1002/jcp.20528

1125 Harrison D. A., P. E. McCoon, R. Binari, M. Gilman, and N. Perrimon, 1998 Drosophila unpaired encodes
1126 a secreted protein that activates the JAK signaling pathway. Gene Dev 12: 3252--3263.
1127 https://doi.org/10.1101/gad.12.20.3252

1128 Hatini V., E. Kula-Eversole, D. Nusinow, and S. J. D. Signore, 2013 Essential roles for stat92E in
1129 expanding and patterning the proximodistal axis of the Drosophila wing imaginal disc. Dev Biol 378:
1130 38--50. https://doi.org/10.1016/j.ydbio.2013.02.016

1131 He N., N. S. Jahchan, E. Hong, Q. Li, M. A. Bayfield, *et al.*, 2008 A La-Related Protein Modulates 7SK
1132 snRNP Integrity to Suppress P-TEFb-Dependent Transcriptional Elongation and Tumorigenesis. Mol
1133 Cell 29: 588–599. https://doi.org/10.1016/j.molcel.2008.01.003

1134 Herreweghe E. V., S. Egloff, I. Goiffon, B. E. Jády, C. Froment, *et al.*, 2007 Dynamic remodelling of
1135 human 7SK snRNP controls the nuclear level of active P-TEFb. Embo J 26: 3570–3580.
1136 https://doi.org/10.1038/sj.emboj.7601783

1137 Hildebrand A., M. Remmert, A. Biegert, and J. Söding, 2009 Fast and accurate automatic structure
1138 prediction with HHpred. Proteins Struct Funct Bioinform 77: 128–132.
1139 https://doi.org/10.1002/prot.22499

1140 Irizarry J., and A. Stathopoulos, 2015 FGF signaling supports Drosophila fertility by regulating
1141 development of ovarian muscle tissues. Dev Biol 404: 1–13.
1142 https://doi.org/10.1016/j.ydbio.2015.04.023

1143 Jeronimo C., D. Forget, A. Bouchard, Q. Li, G. Chua, *et al.*, 2007 Systematic Analysis of the Protein
1144 Interaction Network for the Human Transcription Machinery Reveals the Identity of the 7SK Capping
1145 Enzyme. Mol Cell 27: 262–274. https://doi.org/10.1016/j.molcel.2007.06.027

1146 Johnstone K., R. E. Wells, D. Strutt, and M. P. Zeidler, 2013 Localised JAK/STAT Pathway Activation Is
1147 Required for Drosophila Wing Hinge Development. Plos One 8.
1148 https://doi.org/10.1371/journal.pone.0065076

1149 Jonkers I., and J. T. Lis, 2015 Getting up to speed with transcription elongation by RNA polymerase II.
1150 Nat Rev Mol Cell Bio 16: 167–177. https://doi.org/10.1038/nrm3953

1151 Kairamkonda S., and U. Nongthomba, 2014 Beadex Function in the Motor Neurons Is Essential for
1152 Female Reproduction in Drosophila melanogaster. Plos One 9: e113003.
1153 https://doi.org/10.1371/journal.pone.0113003

1154 Kan L., A. V. Grozhik, J. Vedanayagam, D. P. Patil, N. Pang, *et al.*, 2017 The m6A pathway facilitates sex
1155 determination in Drosophila. Nat Commun 8: 1--16. https://doi.org/10.1038/ncomms15737

1156 Krueger B. J., C. Jeronimo, B. B. Roy, A. Bouchard, C. Barrandon, *et al.*, 2008 LARP7 is a stable
1157 component of the 7SK snRNP while P-TEFb, HEXIM1 and hnRNP A1 are reversibly associated.
1158 Nucleic Acids Res 36: 2219–2229. https://doi.org/10.1093/nar/gkn061

1159 Krueger B. J., K. Varzavand, J. J. Cooper, and D. H. Price, 2010 The Mechanism of Release of P-TEFb
1160 and HEXIM1 from the 7SK snRNP by Viral and Cellular Activators Includes a Conformational Change
1161 in 7SK. Plos One 5: e12335. https://doi.org/10.1371/journal.pone.0012335

1162 Lee P.-T., J. Zirin, O. Kanca, W.-W. Lin, K. L. Schulze, *et al.*, 2018 A gene-specific T2A-GAL4 library for
1163 Drosophila. Elife 7: e35574. https://doi.org/10.7554/elife.35574

1164 Lee S., H. Liu, R. Hill, C. Chen, X. Hong, *et al.*, 2020 JMJD6 cleaves MePCE to release positive
1165 transcription elongation factor b (P-TEFb) in higher eukaryotes. Elife 9: e53930.
1166 https://doi.org/10.7554/elife.53930

1167 Leger A., P. P. Amaral, L. Pandolfini, C. Capitanchik, F. Capraro, *et al.*, 2021 RNA modifications
1168 detection by comparative Nanopore direct RNA sequencing. Nat Commun 12: 7198.
1169 https://doi.org/10.1038/s41467-021-27393-3

1170 Lemieux B., M. Blanchette, A. Monette, A. J. Mouland, R. J. Wellinger, *et al.*, 2015 A Function for the
1171 hnRNP A1/A2 Proteins in Transcription Elongation. Plos One 10: e0126654.
1172 https://doi.org/10.1371/journal.pone.0126654

1173 Lence T., J. Akhtar, M. Bayer, K. Schmid, L. Spindler, *et al.*, 2016 m6A modulates neuronal functions
1174 and sex determination in Drosophila. Nature 540: 242–247. https://doi.org/10.1038/nature20568

1175 Lence T., C. Paolantoni, L. Worpenberg, and J.-Y. Roignant, 2018 Mechanistic insights into m6A RNA
1176 enzymes. Biochimica Et Biophysica Acta Gene Regul Mech.
1177 https://doi.org/10.1016/j.bbagrm.2018.10.014

1178 Levine M., 2011 Paused RNA Polymerase II as a Developmental Checkpoint. Cell 145: 502–511.
1179 https://doi.org/10.1016/j.cell.2011.04.021

1180 Li Q., J. P. Price, S. A. Byers, D. Cheng, J. Peng, *et al.*, 2005 Analysis of the Large Inactive P-TEFb
1181 Complex Indicates That It Contains One 7SK Molecule, a Dimer of HEXIM1 or HEXIM2, and Two P-
1182 TEFb Molecules Containing Cdk9 Phosphorylated at Threonine 186*. J Biol Chem 280: 28819–
1183 28826. https://doi.org/10.1074/jbc.m502712200

1184 Li J., and D. S. Gilmour, 2011 Promoter proximal pausing and the control of gene expression. Curr Opin
1185 Genet Dev 21: 231–235. https://doi.org/10.1016/j.gde.2011.01.010

1186 Liao S., and D. R. Nässel, 2020 Drosophila Insulin-Like Peptide 8 (DILP8) in Ovarian Follicle Cells
1187 Regulates Ovulation and Metabolism. Front Endocrinol 11: 461.
1188 https://doi.org/10.3389/fendo.2020.00461

1189 Liu X., W. L. Kraus, and X. Bai, 2015 Ready, pause, go: regulation of RNA polymerase II pausing and
1190 release by cellular signaling pathways. Trends Biochem Sci 40: 516–525.
1191 https://doi.org/10.1016/j.tibs.2015.07.003

1192 Lobell A. S., R. R. Kaspari, Y. L. S. Negron, and S. T. Harbison, 2017 The Genetic Architecture of
1193 Ovariole Number in Drosophila melanogaster: Genes with Major, Quantitative, and Pleiotropic
1194 Effects. G3 Genes Genomes Genetics 7: 2391–2403. https://doi.org/10.1534/g3.117.042390

1195 Maimon I., and L. Gilboa, 2011 Dissection and Staining of Drosophila Larval Ovaries. J Vis
1196 Exp. https://doi.org/10.3791/2537

1197 Manjila S., and G. Hasan, 2018 Flight and Climbing Assay for Assessing Motor Functions in Drosophila.
1198 Bio-protocol 8. https://doi.org/10.21769/bioprotoc.2742

1199 Margaritis T., and F. C. P. Holstege, 2008 Poised RNA Polymerase II Gives Pause for Thought. Cell 133:
1200 581–584. https://doi.org/10.1016/j.cell.2008.04.027

1201 Markert A., M. Grimm, J. Martinez, J. Wiesner, A. Meyerhans, *et al.*, 2008 The La-related protein LARP7
1202 is a component of the 7SK ribonucleoprotein and affects transcription of cellular and viral
1203 polymerase II genes. Embo Rep 9: 569–575. https://doi.org/10.1038/embor.2008.72

1204 Marshall N. F., and D. H. Price, 1995 Purification of P-TEFb, a Transcription Factor Required for the
1205 Transition into Productive Elongation (∗). J Biol Chem 270: 12335–12338.
1206 https://doi.org/10.1074/jbc.270.21.12335

1207 Marshall N. F., J. Peng, Z. Xie, and D. H. Price, 1996 Control of RNA Polymerase II Elongation Potential
1208 by a Novel Carboxyl-terminal Domain Kinase*. J Biol Chem 271: 27176–27183.
1209 https://doi.org/10.1074/jbc.271.43.27176

1210 Mayer A., H. M. Landry, and L. S. Churchman, 2017 Pause & go: from the discovery of RNA polymerase
1211 pausing to its functional implications. Curr Opin Cell Biol 46: 72–80.
1212 https://doi.org/10.1016/j.ceb.2017.03.002

1213 Meier A., and J. Söding, 2015 Automatic Prediction of Protein 3D Structures by Probabilistic Multi-
1214 template Homology Modeling. Plos Comput Biol 11: e1004343.
1215 https://doi.org/10.1371/journal.pcbi.1004343

1216 Mészáros B., G. Erdős, and Z. Dosztányi, 2018 IUPred2A: context-dependent prediction of protein
1217 disorder as a function of redox state and protein binding. Nucleic Acids Res 46: gky384-.
1218 https://doi.org/10.1093/nar/gky384

1219 Michels A. A., A. Fraldi, Q. Li, T. E. Adamson, F. Bonnet, *et al.*, 2004 Binding of the 7SK snRNA turns the
1220 HEXIM1 protein into a P-TEFb (CDK9/cyclin T) inhibitor. Embo J 23: 2608–2619.
1221 https://doi.org/10.1038/sj.emboj.7600275

1222 Muniz L., S. Egloff, and T. Kiss, 2013 RNA elements directing in vivo assembly of the 7SK/MePCE/Larp7
1223 transcriptional regulatory snRNP. Nucleic Acids Res 41: 4686–4698.
1224 https://doi.org/10.1093/nar/gkt159

1225 Murphy S., M. Tripodi, and M. Melli, 1986 A sequence upstream from the coding region is required for
1226 the transcription of the 7SK RNA genes. Nucleic Acids Res 14: 9243–9260.
1227 https://doi.org/10.1093/nar/14.23.9243

1228 Murphy S., C. D. Liegro, and M. Melli, 1987 The in vitro transcription of the 7SK RNA gene by RNA
1229 polymerase III is dependent only on the presence of an upstream promoter. Cell 51: 81–87.
1230 https://doi.org/10.1016/0092-8674(87)90012-2

1231 Murphy S., A. Pierani, C. Scheidereit, M. Melli, and R. G. Roeder, 1989 Purified octamer binding
1232 transcription factors stimulate RNA polymerase III-mediated transcription of the 7SK RNA gene. Cell
1233 59: 1071–1080. https://doi.org/10.1016/0092-8674(89)90763-0

1234 Nechaev S., and K. Adelman, 2011 Pol II waiting in the starting gates: Regulating the transition from
1235 transcription initiation into productive elongation. Biochimica Et Biophysica Acta Bba - Gene Regul
1236 Mech 1809: 34–45. https://doi.org/10.1016/j.bbagrm.2010.11.001

1237 Nguyen V. T., T. Kiss, A. A. Michels, and O. Bensaude, 2001 7SK small nuclear RNA binds to and inhibits
1238 the activity of CDK9/cyclin T complexes. Nature 414: 322–325. https://doi.org/10.1038/35104581

1239 Nguyen D., B. J. Krueger, S. C. Sedore, J. E. Brogie, J. T. Rogers, *et al.*, 2012 The Drosophila 7SK snRNP
1240 and the essential role of dHEXIM in development. Nucleic Acids Res 40: 5283–5297.
1241 https://doi.org/10.1093/nar/gks191

1242 Ni Z., B. E. Schwartz, J. Werner, J.-R. Suarez, and J. T. Lis, 2004 Coordination of Transcription, RNA
1243 Processing, and Surveillance by P-TEFb Kinase on Heat Shock Genes. Mol Cell 13: 55–65.
1244 https://doi.org/10.1016/s1097-2765(03)00526-4

1245 Ni Z., A. Saunders, N. J. Fuda, J. Yao, J.-R. Suarez, *et al.*, 2008 P-TEFb Is Critical for the Maturation of
1246 RNA Polymerase II into Productive Elongation In Vivo. Mol Cell Biol 28: 1161–1170.
1247 https://doi.org/10.1128/mcb.01859-07

1248 Ni J. Q., R. Zhou, B. Czech, L. P. Liu, L. Holderbaum, *et al.*, 2011 A genome-scale shRNA resource for
1249 transgenic RNAi in Drosophila. Nat Methods 8: 405--407. https://doi.org/10.1038/nmeth.1592

1250 Niessing D., N. Dostatni, H. Jäckle, and R. Rivera-Pomar, 1999 Sequence interval within the PEST motif
1251 of Bicoid is important for translational repression of caudal mRNA in the anterior region of the
1252 Drosophila embryo. Embo J 18: 1966–1973. https://doi.org/10.1093/emboj/18.7.1966

1253 Niessing D., W. Driever, F. Sprenger, H. Taubert, H. Jäckle, *et al.*, 2000 Homeodomain Position 54
1254 Specifies Transcriptional versus Translational Control by Bicoid. Mol Cell 5: 395–401.
1255 https://doi.org/10.1016/s1097-2765(00)80434-7

1256 Niessing D., S. Blanke, and H. Jäckle, 2002 Bicoid associates with the 5′-cap-bound complex of caudal
1257 mRNA and represses translation. Gene Dev 16: 2576–2582. https://doi.org/10.1101/gad.240002

1258 Páez-Moscoso D. J., D. V. Ho, L. Pan, K. Hildebrand, K. L. Jensen, *et al.*, 2022 A putative cap binding
1259 protein and the methyl phosphate capping enzyme Bin3/MePCE function in telomerase biogenesis.
1260 Nat Commun 13: 1067. https://doi.org/10.1038/s41467-022-28545-9

1261 Parks A. L., K. R. Cook, M. Belvin, N. A. Dompe, R. Fawcett, *et al.*, 2004 Systematic generation of high-
1262 resolution deletion coverage of the Drosophila melanogaster genome. Nat Genet 36: 288--292.
1263 https://doi.org/10.1038/ng1312

1264 Peng J., N. F. Marshall, and D. H. Price, 1998 Identification of a Cyclin Subunit Required for the Function
1265 ofDrosophila P-TEFb*. J Biol Chem 273: 13855–13860. https://doi.org/10.1074/jbc.273.22.13855

1266 Perez-Pepe M., A. W. Desotell, H. Li, W. Li, B. Han, *et al.*, 2023 7SK methylation by METTL3 promotes
1267 transcriptional activity. Sci Adv 9. https://doi.org/10.1126/sciadv.ade7500

1268 Peterlin B. M., J. E. Brogie, and D. H. Price, 2011 7SK snRNA: a noncoding RNA that plays a major role in
1269 regulating eukaryotic transcription. Wiley Interdiscip Rev Rna 3: 92–103.
1270 https://doi.org/10.1002/wrna.106

1271 Pfeiffer B. D., A. Jenett, A. S. Hammonds, T.-T. B. Ngo, S. Misra, *et al.*, 2008 Tools for neuroanatomy
1272 and neurogenetics in Drosophila. Proc National Acad Sci 105: 9715–9720.
1273 https://doi.org/10.1073/pnas.0803697105

1274 Porat J., M. E. Baidouri, J. Grigull, J.-M. Deragon, and M. A. Bayfield, 2022 The methyl phosphate
1275 capping enzyme Bmc1/Bin3 is a stable component of the fission yeast telomerase holoenzyme. Nat
1276 Commun 13: 1277. https://doi.org/10.1038/s41467-022-28985-3

1277 Qiao H. H., F. Wang, R. G. Xu, J. Sun, R. Zhu, *et al.*, 2018 An efficient and multiple target transgenic
1278 RNAi technique with low toxicity in Drosophila. Nat Commun 9. https://doi.org/10.1038/s41467-018-
1279 06537-y

1280 Raj A., and S. Tyagi, 2010 Single Molecule Tools: Fluorescence Based Approaches, Part A. Methods
1281 Enzymol 472: 365–386. https://doi.org/10.1016/s0076-6879(10)72004-8

1282 Ramanathan Y., S. M. Rajpara, S. M. Reza, E. Lees, S. Shuman, *et al.*, 2001 Three RNA Polymerase II
1283 Carboxyl-terminal Domain Kinases Display Distinct Substrate Preferences*. J Biol Chem 276: 10913–
1284 10920. https://doi.org/10.1074/jbc.m010975200

1285 Rivera-Pomar R., D. Niessing, U. Schmidt-Ott, W. J. Gehring, and H. Jäckle, 1996 RNA binding and
1286 translational suppression by bicoid. Nature 379: 746–9. https://doi.org/10.1038/379746a0

1287 Ryder E., F. Blows, M. Ashburner, R. Bautista-Llacer, D. Coulson, *et al.*, 2004 The DrosDel collection: A
1288 set of P-element insertions for generating custom chromosomal aberrations in Drosophila
1289 melanogaster. Genetics 167: 797--813. https://doi.org/10.1534/genetics.104.026658

1290 Sahut-Barnola I., D. Godt, F. A. Laski, and J.-L. Couderc, 1995 Drosophila Ovary Morphogenesis:
1291 Analysis of Terminal Filament Formation and Identification of a Gene Required for This Process. Dev
1292 Biol 170: 127–135. https://doi.org/10.1006/dbio.1995.1201

1293 Sahut-Barnola I., B. Dastugue, and J.-L. Couderc, 1996 Terminal filament cell organization in the larval
1294 ovary of Drosophila melanogaster: ultrastructural observations and pattern of divisions. Roux's
1295 Archives Dev Biology 205: 356–363. https://doi.org/10.1007/bf00377215

1296 Šali A., L. Potterton, F. Yuan, H. van Vlijmen, and M. Karplus, 1995 Evaluation of comparative protein
1297 modeling by MODELLER. Proteins Struct Funct Bioinform 23: 318–326.
1298 https://doi.org/10.1002/prot.340230306

1299 Sanhueza M., L. Zechini, T. Gillespie, and G. Pennetta, 2014 Gain-of-function mutations in the ALS8
1300 causative gene VAPB have detrimental effects on neurons and muscles. Biol Open 3: 59--71.
1301 https://doi.org/10.1242/bio.20137070

1302 Schneeberger P. E., T. Bierhals, A. Neu, M. Hempel, and K. Kutsche, 2019 de novo MEPCE nonsense
1303 variant associated with a neurodevelopmental disorder causes disintegration of 7SK snRNP and
1304 enhanced RNA polymerase II activation. Sci Rep-uk 9: 12516. https://doi.org/10.1038/s41598-019-
1305 49032-0

1306 Shelton S. B., N. M. Shah, N. S. Abell, S. K. Devanathan, M. Mercado, *et al.*, 2018 Crosstalk between the
1307 RNA Methylation and Histone-Binding Activities of MePCE Regulates P-TEFb Activation on
1308 Chromatin. Cell Reports 22: 1374–1383. https://doi.org/10.1016/j.celrep.2018.01.028

1309 Shim E. Y., A. K. Walker, Y. Shi, and T. K. Blackwell, 2002 CDK-9/cyclin T (P-TEFb) is required in two
1310 postinitiation pathways for transcription in the C. elegans embryo. Gene Dev 16: 2135–2146.
1311 https://doi.org/10.1101/gad.999002

1312 Shimba S., and R. Reddy, 1994 Purification of human U6 small nuclear RNA capping enzyme. Evidence
1313 for a common capping enzyme for gamma-monomethyl-capped small RNAs. J Biological Chem 269:
1314 12419–23.

1315 Shukla V., F. Habib, A. Kulkarni, and G. S. Ratnaparkhi, 2013 Gene Duplication, Lineage-Specific
1316 Expansion, and Subfunctionalization in the MADF-BESS Family Patterns the Drosophila Wing
1317 Hinge. Genetics 196: 481–496. https://doi.org/10.1534/genetics.113.160531

1318 Shumyatsky G. P., S. V. Tillib, and D. A. Kramerov, 1990 B2 RNA and 7SK RNA, RNA polymerase III
1319 transcripts, have a cap-like structure at their 5′ end. Nucleic Acids Res 18: 6347–6351.
1320 https://doi.org/10.1093/nar/18.21.6347

1321 Shumyatsky G., D. Wright, and R. Reddy, 1993 Methylphosphate cap structure increases the stability of
1322 7SK, B2 and U6 small RNAs in Xenopus oocytes. Nucleic Acids Res 21: 4756–4761.
1323 https://doi.org/10.1093/nar/21.20.4756

1324 Shumyatsky G., S. Shimba, and R. Reddy, 1994 Capping signals correspond to the 5′ end in four
1325 eukaryotic small RNAs containing gamma-monomethylphosphate cap structure. Gene Expression
1326 4: 29--41.

1327 Singh R., S. Gupta, and R. Reddy, 1990 Capping of Mammalian U6 Small Nuclear RNA In Vitro Is
1328 Directed by a Conserved Stem-Loop and AUAUAC Sequence: Conversion of a Noncapped RNA into
1329 a Capped RNA. Mol Cell Biol 10: 939–946. https://doi.org/10.1128/mcb.10.3.939-946.1990

1330 Singh N., H. Morlock, and S. D. Hanes, 2011 The Bin3 RNA methyltransferase is required for repression
1331 of caudal translation in the Drosophila embryo. Dev Biol 352: 104–115.
1332 https://doi.org/10.1016/j.ydbio.2011.01.017

1333 Söding J., 2005 Protein homology detection by HMM–HMM comparison. Bioinformatics 21: 951–960.
1334 https://doi.org/10.1093/bioinformatics/bti125

1335 Spradling A. C., D. Stern, A. Beaton, E. J. Rhem, T. Laverty, *et al.*, 1999 The Berkeley Drosophila
1336 Genome Project Gene Disruption Project: Single P-Element Insertions Mutating 25% of Vital
1337 Drosophila Genes. Genetics 153: 135–177. https://doi.org/10.1093/genetics/153.1.135

1338 Takeo S., S. K. Swanson, K. Nandanan, Y. Nakai, T. Aigaki, *et al.*, 2012 Shaggy/glycogen synthase
1339 kinase 3β and phosphorylation of Sarah/regulator of calcineurin are essential for completion of
1340 Drosophila female meiosis. Proc National Acad Sci 109: 6382–6389.
1341 https://doi.org/10.1073/pnas.1120367109

1342 Wada T., T. Takagi, Y. Yamaguchi, D. Watanabe, and H. Handa, 1998 Evidence that P-TEFb alleviates
1343 the negative effect of DSIF on RNA polymerase II-dependent transcription in vitro. Embo J 17: 7395–
1344 7403. https://doi.org/10.1093/emboj/17.24.7395

1345 Wang X., S. Hang, L. Prazak, and J. P. Gergen, 2010 NELF Potentiates Gene Transcription in the
1346 Drosophila Embryo. Plos One 5: e11498. https://doi.org/10.1371/journal.pone.0011498

1347 Wang S., P. Chai, R. Jia, and R. Jia, 2018 Novel insights on m6A RNA methylation in tumorigenesis: a
1348 double-edged sword. Mol Cancer 17: 101. https://doi.org/10.1186/s12943-018-0847-4

1349 Wang F., H.-H. Qiao, R.-G. Xu, J. Sun, R. Zhu, *et al.*, 2019 pNP Transgenic RNAi System Manual in
1350 Drosophila. Bio-protocol 9: 1--12. https://doi.org/10.21769/bioprotoc.3158

1351 Warda A. S., J. Kretschmer, P. Hackert, C. Lenz, H. Urlaub, *et al.*, 2017 Human METTL16 is a N6-
1352 methyladenosine (m6A) methyltransferase that targets pre-mRNAs and various non-coding RNAs.
1353 Embo Rep 18: 2004–2014. https://doi.org/10.15252/embr.201744940

1354 Wayne M. L., J. B. Hackett, and T. F. C. Mackay, 1997 QUANTITATIVE GENETICS OF OVARIOLE
1355 NUMBER IN DROSOPHILA MELANOGASTER. I. SEGREGATING VARIATION AND FITNESS.
1356 Evolution 51: 1156–1163. https://doi.org/10.1111/j.1558-5646.1997.tb03963.x

1357 Wayne M. L., and T. F. C. Mackay, 1998 Quantitative Genetics of Ovariole Number in Drosophila
1358 melanogaster. II. Mutational Variation and Genotype-Environment Interaction. Genetics 148: 201–
1359 210. https://doi.org/10.1093/genetics/148.1.201

1360 Xu X., L. Ma, X. Zhang, S. Guo, W. Guo, *et al.*, 2022 A positive feedback circuit between RN7SK snRNA
1361 and m6A readers is essential for tumorigenesis. Mol Ther J Am Soc Gene Ther.
1362 https://doi.org/10.1016/j.ymthe.2022.12.013

1363 Xue Y., Z. Yang, R. Chen, and Q. Zhou, 2010 A capping-independent function of MePCE in stabilizing
1364 7SK snRNA and facilitating the assembly of 7SK snRNP. Nucleic Acids Res 38: 360–369.
1365 https://doi.org/10.1093/nar/gkp977

1366 Yamaguchi Y., T. Takagi, T. Wada, K. Yano, A. Furuya, *et al.*, 1999 NELF, a Multisubunit Complex
1367 Containing RD, Cooperates with DSIF to Repress RNA Polymerase II Elongation. Cell 97: 41–51.
1368 https://doi.org/10.1016/s0092-8674(00)80713-8

1369 Yang Z., Q. Zhu, K. Luo, and Q. Zhou, 2001 The 7SK small nuclear RNA inhibits the CDK9/cyclin T1
1370 kinase to control transcription. Nature 414: 317–322. https://doi.org/10.1038/35104575

1371 Yang Y., C. D. Eichhorn, Y. Wang, D. Cascio, and J. Feigon, 2019 Structural basis of 7SK RNA 5′-γ-
1372 phosphate methylation and retention by MePCE. Nat Chem Biol 15: 132–140.
1373 https://doi.org/10.1038/s41589-018-0188-z

1374 Yang Y., S. Liu, S. Egloff, C. D. Eichhorn, T. Hadjian, *et al.*, 2022 Structural basis of RNA conformational
1375 switching in the transcriptional regulator 7SK RNP. Mol Cell 82: 1724-1736.e7.
1376 https://doi.org/10.1016/j.molcel.2022.03.001

1377 Yik J. H. N., R. Chen, A. C. Pezda, C. S. Samford, and Q. Zhou, 2004 A Human Immunodeficiency Virus
1378 Type 1 Tat-Like Arginine-Rich RNA-Binding Domain Is Essential for HEXIM1 To Inhibit RNA
1379 Polymerase II Transcription through 7SK snRNA-Mediated Inactivation of P-TEFb. Mol Cell Biol 24:
1380 5094–5105. https://doi.org/10.1128/mcb.24.12.5094-5105.2004

1381 Zhang B., Z. Liu, J. Liu, K. Cao, W. Shan, *et al.*, 2021 Long non-coding RNA ST8SIA6-AS1 promotes the
1382 migration and invasion of hypoxia-treated hepatocellular carcinoma cells through the miR-
1383 338/MEPCE axis. Oncol Rep 45: 73–82. https://doi.org/10.3892/or.2020.7864

1384 Zhou M., M. A. Halanski, M. F. Radonovich, F. Kashanchi, J. Peng, *et al.*, 2000 Tat Modifies the Activity
1385 of CDK9 To Phosphorylate Serine 5 of the RNA Polymerase II Carboxyl-Terminal Domain during

1386 Human Immunodeficiency Virus Type 1 Transcription. Mol Cell Biol 20: 5077–5086.
1387 https://doi.org/10.1128/mcb.20.14.5077-5086.2000

1388 Zhou Q., T. Li, and D. H. Price, 2012 RNA Polymerase II Elongation Control. Biochemistry-us 81: 119–
1389 143. https://doi.org/10.1146/annurev-biochem-052610-095910

1390 Zhu W., and S. D. Hanes, 2000 Identification of Drosophila Bicoid-interacting proteins using a custom
1391 two-hybrid selection. Gene 245: 329–339. https://doi.org/10.1016/s0378-1119(00)00048-2

1392 Zieve G., and S. Penman, 1976 Small RNA species of the HeLa cell: Metabolism and subcellular
1393 localization. Cell 8: 19–31. https://doi.org/10.1016/0092-8674(76)90181-1

1394 Zimmermann L., A. Stephens, S.-Z. Nam, D. Rau, J. Kübler, *et al.*, 2018 A Completely Reimplemented
1395 MPI Bioinformatics Toolkit with a New HHpred Server at its Core. J Mol Biol 430: 2237–2243.
1396 https://doi.org/10.1016/j.jmb.2017.12.007

Fig. 1

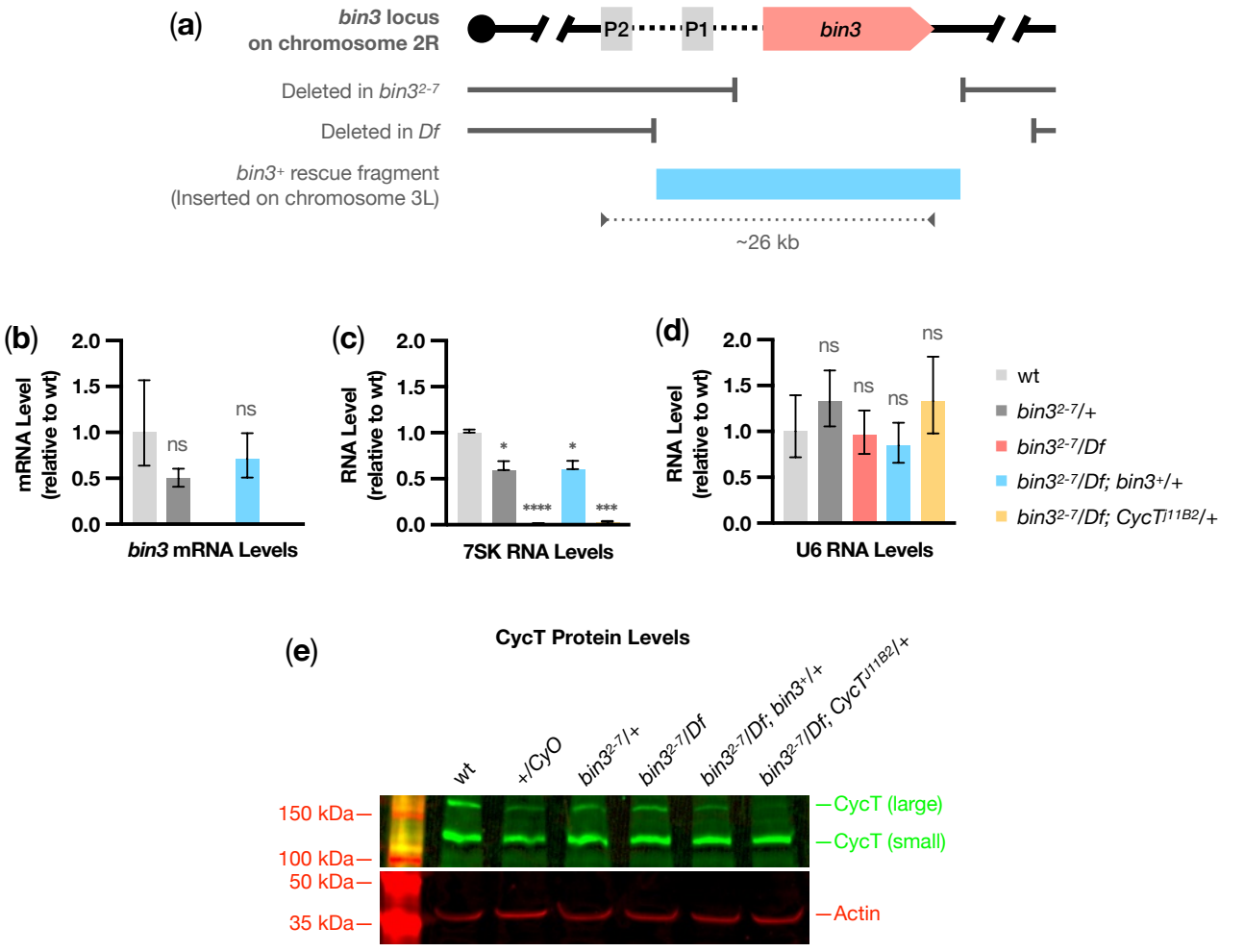
(a)
bin3 locus on chromosome 2R
P2
P1
bin3
Deleted in bin3 2-7
Deleted in Df
bin3+ rescue fragment (Inserted on chromosome 3L)
~26 kb
(b)
mRNA Level (relative to wt)
2.0
1.5
1.0
0.5
0.0
ns
ns
bin3 mRNA Levels
(c)
RNA Level (relative to wt)
*
****
*
***
7SK RNA Levels
(d)
RNA Level (relative to wt)
ns
ns
ns
ns
U6 RNA Levels
wt
bin3 2-7/+
bin3 2-7/Df
bin3 2-7/Df; bin3+/+
bin3 2-7/Df; CycT J11B2/+
(e)
CycT Protein Levels
wt
+/CyO
bin3 2-7/+
bin3 2-7/Df
bin3 2-7/Df; bin3+/+
bin3 2-7/Df; CycT J11B2/+
150 kDa
100 kDa
50 kDa
35 kDa
CycT (large)
CycT (small)
Actin

Fig. 2

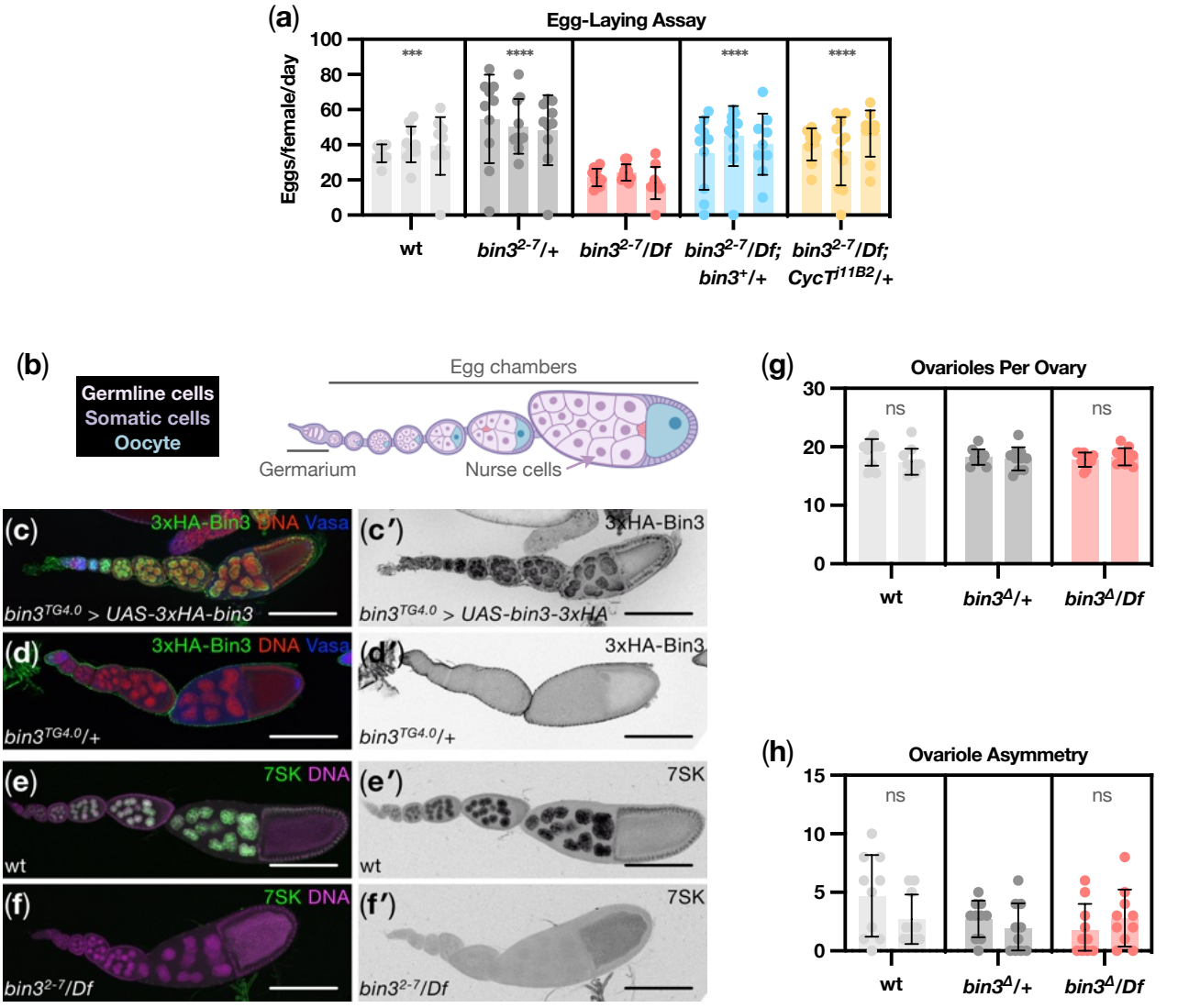
(a)
Egg-Laying Assay
Eggs/female/day
100
80
60
40
20
0
***
****
****
****
wt
bin3^2-7/+
bin3^2-7/Df
bin3^2-7/Df; bin3^+/+
bin3^2-7/Df; CycT^j11B2/+
(b)
Germline cells
Somatic cells
Oocyte
Egg chambers
Germarium
Nurse cells
(c)
3xHA-Bin3 DNA Vasa
bin3^TG4.0 > UAS-3xHA-bin3
(c′)
3xHA-Bin3
bin3^TG4.0 > UAS-bin3-3xHA
(d)
3xHA-Bin3 DNA Vasa
bin3^TG4.0/+
(d′)
3xHA-Bin3
bin3^TG4.0/+
(e)
7SK DNA
wt
(e′)
7SK
wt
(f)
7SK DNA
bin3^2-7/Df
(f′)
7SK
bin3^2-7/Df
(g)
Ovarioles Per Ovary
30
20
10
0
ns
ns
wt
bin3^Δ/+
bin3^Δ/Df
(h)
Ovariole Asymmetry
15
10
5
0
ns
ns
wt
bin3^Δ/+
bin3^Δ/Df
(i)
Egg-laying Assay with
Germline-Specific Bin3 expression
Eggs/female/day
120
100
80
60
40
20
0
*
***
ns
wt
bin3^2-7/+; nos-GAL4::VP16/+
bin3^2-7/Df; nos-GAL4::VP16/+
bin3^2-7/Df; nos-GAL4::VP16/UAS-bin3

Fig. 3

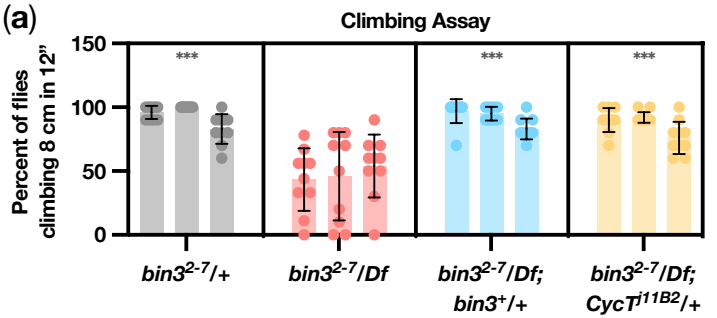
(a)
Climbing Assay
Percent of flies climbing 8 cm in 12"
150
100
50
0
***
***
***
bin3²⁻⁷/+
bin3²⁻⁷/Df
bin3²⁻⁷/Df; bin3⁺/+
bin3²⁻⁷/Df; CycT^j11B2/+

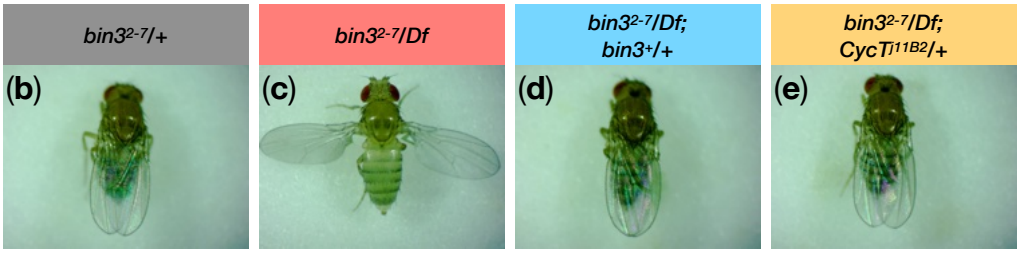
bin3²⁻⁷/+
(b)
bin3²⁻⁷/Df
(c)
bin3²⁻⁷/Df; bin3⁺/+
(d)
bin3²⁻⁷/Df; CycT^j11B2/+
(e)

Fig. 4

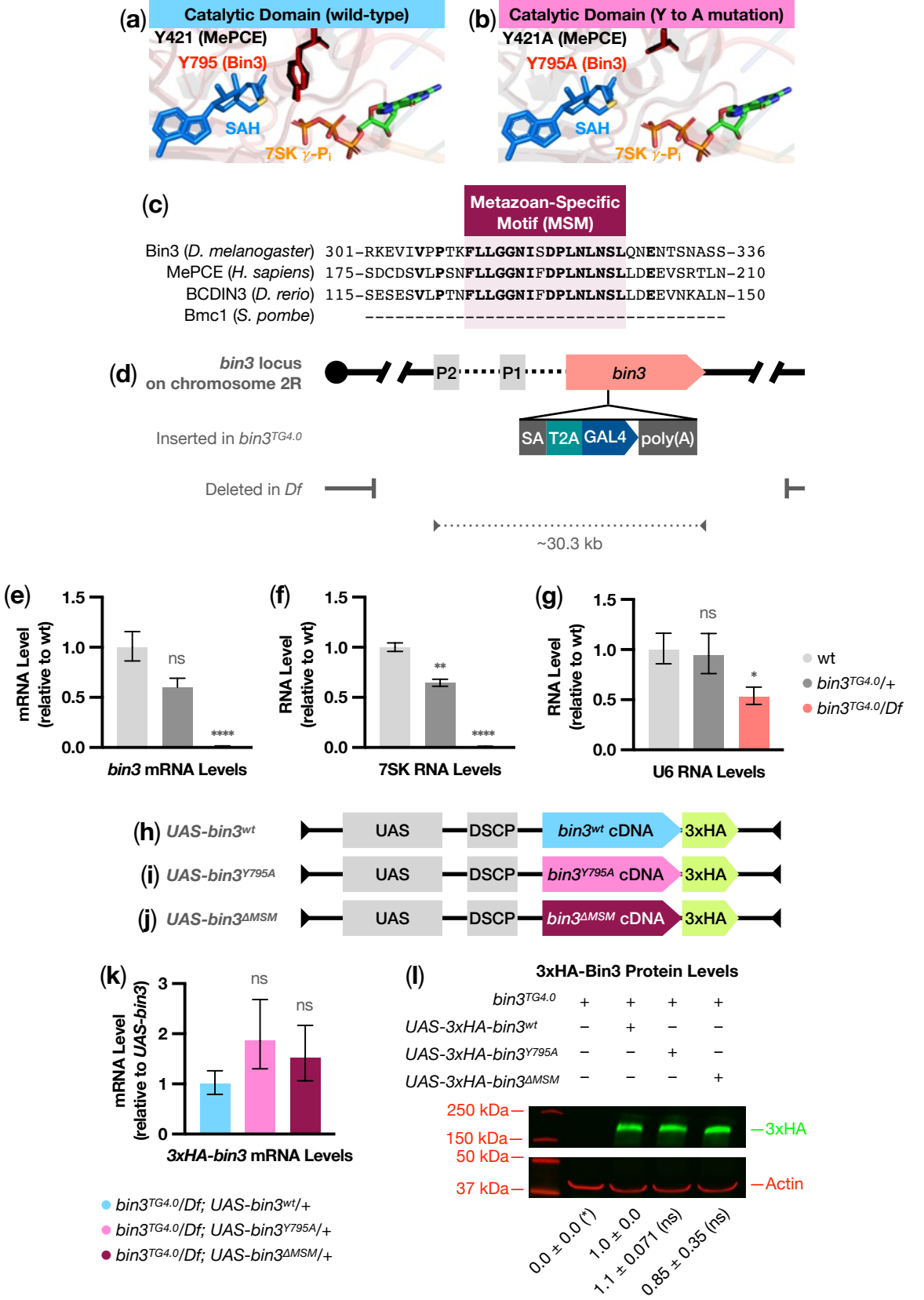
(a)
Catalytic Domain (wild-type)
Y421 (MePCE)
Y795 (Bin3)
SAH
7SK γ-Pi
(b)
Catalytic Domain (Y to A mutation)
Y421A (MePCE)
Y795A (Bin3)
SAH
7SK γ-Pi
(c)
Metazoan-Specific Motif (MSM)
Bin3 (D. melanogaster) 301-RKEVIVPPTKFLLGGNISDPLNLNSLQNENTSNASS-336
MePCE (H. sapiens) 175-SDCDSVLPSNFLLGGNIFDPLNLNSLLDEEVSRTLN-210
BCDIN3 (D. rerio) 115-SESESVLPTNFLLGGNIFDPLNLNSLLDEEVNKALN-150
Bmc1 (S. pombe) ----------
(d)
bin3 locus on chromosome 2R
P2
P1
bin3
Inserted in bin3TG4.0
SA
T2A
GAL4
poly(A)
Deleted in Df
~30.3 kb
(e)
mRNA Level (relative to wt)
1.5
1.0
0.5
0.0
ns
****
bin3 mRNA Levels
(f)
RNA Level (relative to wt)
**
****
7SK RNA Levels
(g)
ns
*
U6 RNA Levels
wt
bin3TG4.0/+
bin3TG4.0/Df
(h) UAS-bin3wt
(i) UAS-bin3Y795A
(j) UAS-bin3ΔMSM
UAS
DSCP
bin3wt cDNA
bin3Y795A cDNA
bin3ΔMSM cDNA
3xHA
(k)
mRNA Level (relative to UAS-bin3)
3
2
1
0
ns
ns
3xHA-bin3 mRNA Levels
bin3TG4.0/Df; UAS-bin3wt/+
bin3TG4.0/Df; UAS-bin3Y795A/+
bin3TG4.0/Df; UAS-bin3ΔMSM/+
(l)
3xHA-Bin3 Protein Levels
bin3TG4.0 + + + +
UAS-3xHA-bin3wt − + − −
UAS-3xHA-bin3Y795A − − + −
UAS-3xHA-bin3ΔMSM − − − +
250 kDa
150 kDa
50 kDa
37 kDa
3xHA
Actin
0.0 ± 0.0 (*)
1.0 ± 0.0
1.1 ± 0.071 (ns)
0.85 ± 0.35 (ns)

Fig. 5

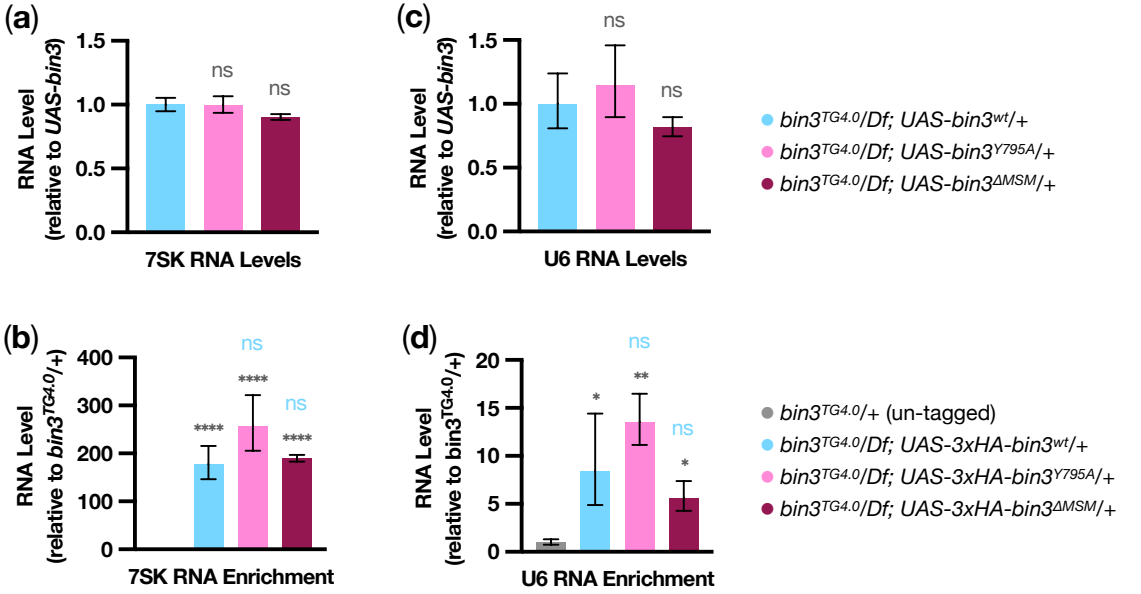
(a)
RNA Level
(relative to UAS-bin3)
1.5
1.0
0.5
0.0
ns
ns
7SK RNA Levels
(c)
RNA Level
(relative to UAS-bin3)
1.5
1.0
0.5
0.0
ns
ns
U6 RNA Levels
bin3TG4.0/Df; UAS-bin3wt/+
bin3TG4.0/Df; UAS-bin3Y795A/+
bin3TG4.0/Df; UAS-bin3ΔMSM/+
(b)
RNA Level
(relative to bin3TG4.0/+)
400
300
200
100
0
ns
****
****
ns
****
7SK RNA Enrichment
(d)
RNA Level
(relative to bin3TG4.0/+)
20
15
10
5
0
ns
*
**
ns
*
U6 RNA Enrichment
bin3TG4.0/+ (un-tagged)
bin3TG4.0/Df; UAS-3xHA-bin3wt/+
bin3TG4.0/Df; UAS-3xHA-bin3Y795A/+
bin3TG4.0/Df; UAS-3xHA-bin3ΔMSM/+

Fig. 6

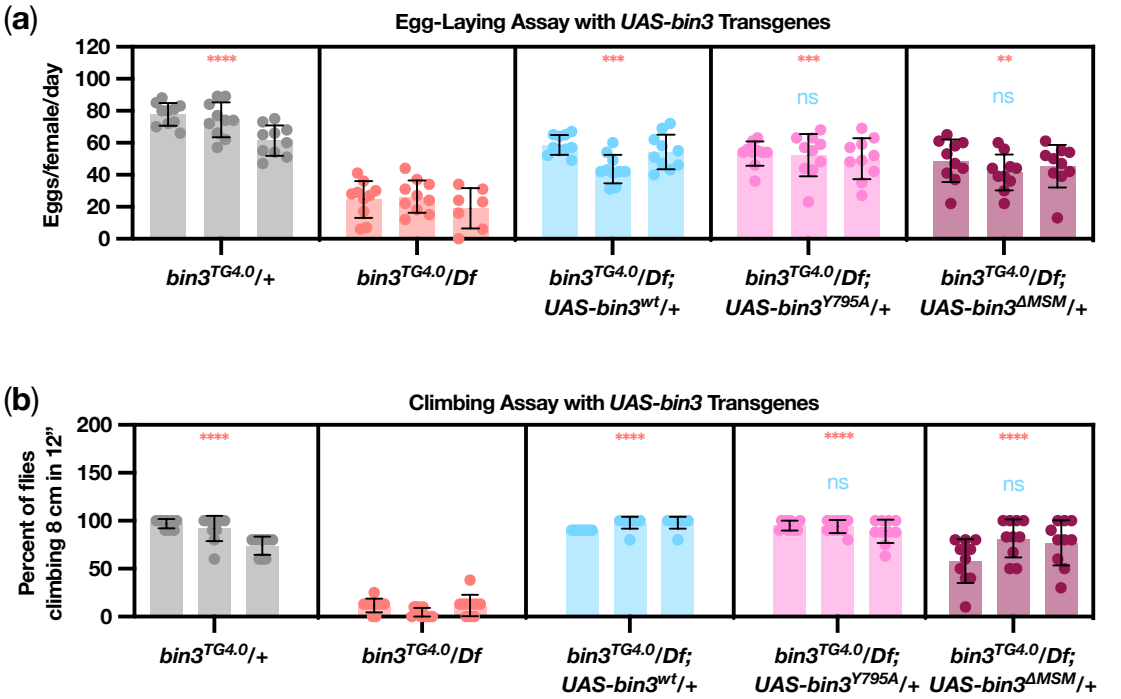
(a)
Egg-Laying Assay with UAS-bin3 Transgenes
Eggs/female/day
120
100
80
60
40
20
0
****
***
***
ns
**
ns
bin3TG4.0/+
bin3TG4.0/Df
bin3TG4.0/Df; UAS-bin3wt/+
bin3TG4.0/Df; UAS-bin3Y795A/+
bin3TG4.0/Df; UAS-bin3ΔMSM/+
(b)
Climbing Assay with UAS-bin3 Transgenes
Percent of flies climbing 8 cm in 12"
200
150
100
50
0
****
****
****
ns
****
ns
bin3TG4.0/+
bin3TG4.0/Df
bin3TG4.0/Df; UAS-bin3wt/+
bin3TG4.0/Df; UAS-bin3Y795A/+
bin3TG4.0/Df; UAS-bin3ΔMSM/+

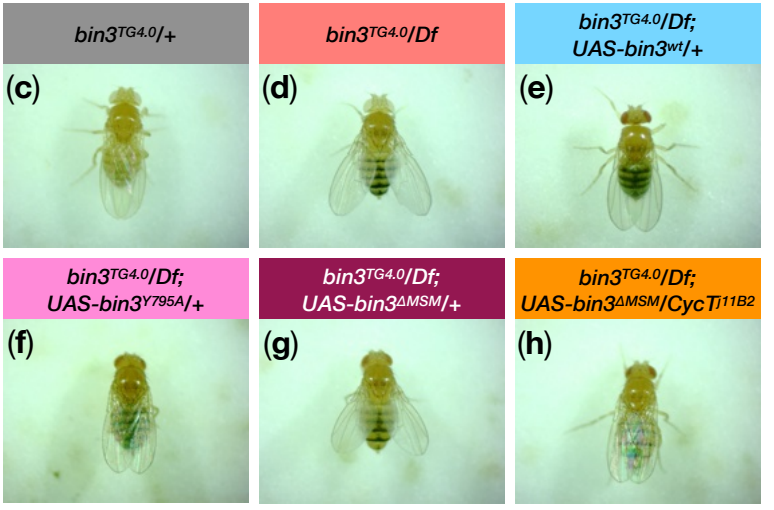
bin3TG4.0/+
(c)
bin3TG4.0/Df
(d)
bin3TG4.0/Df; UAS-bin3wt/+
(e)
bin3TG4.0/Df; UAS-bin3Y795A/+
(f)
bin3TG4.0/Df; UAS-bin3ΔMSM/+
(g)
bin3TG4.0/Df; UAS-bin3ΔMSM/CycTj11B2
(h)

Fig. 7

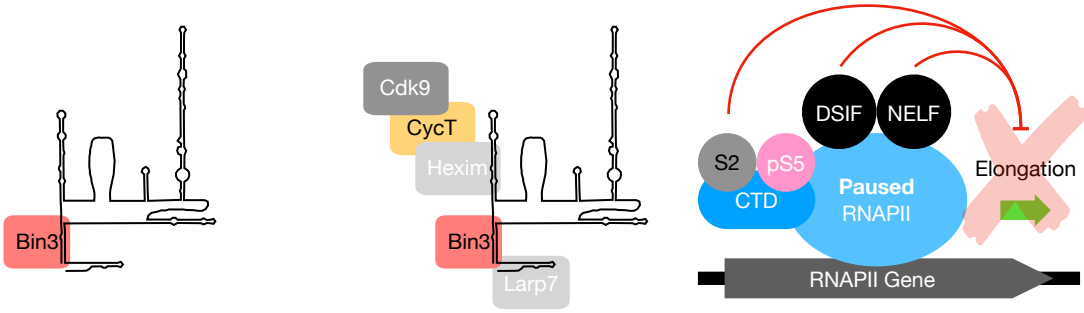

		Bin3 binds 7SK	Bin3 caps 7SK	Bin3 stabilizes 7SK	7SK snRNP assembles and represses P-TEFb	Repressed P-TEFb promotes RNAPII pausing to support…		
						Fecundity	Climbing	Wing posture
(a)	Bin3^{wt}	✓	✓	✓	✓	✓	✓	✓
(b)	Bin3^{Y795A}	✓	✗	✓	✓	✓	✓	✓
(c)	Bin3^{MSM}	✓	✓	✓	✓	✓	✓	✗

Fig. 8

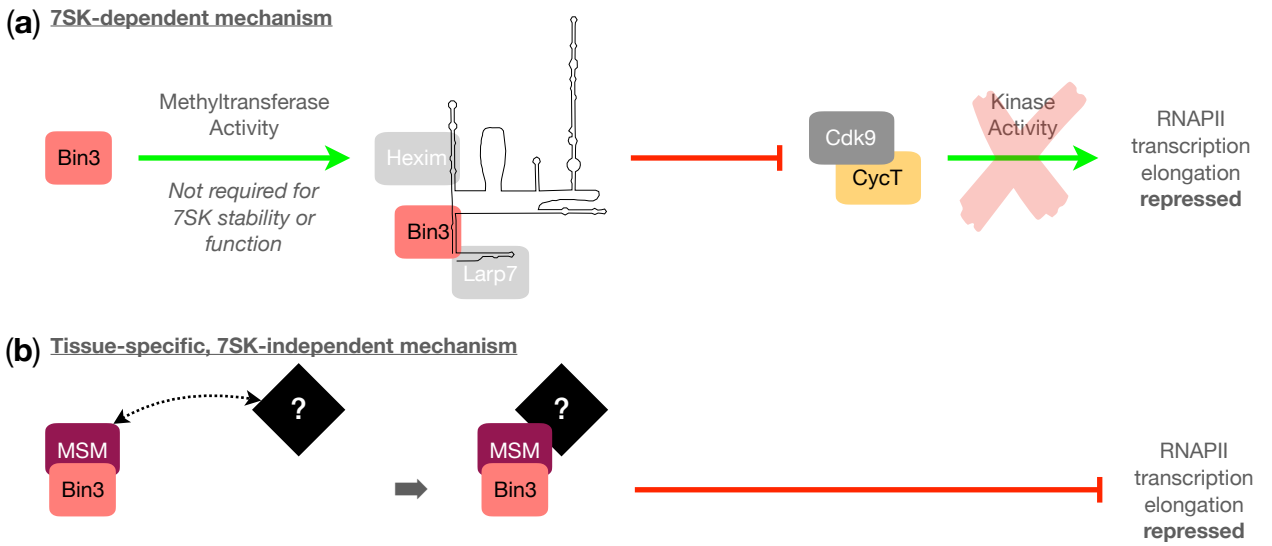
(a) 7SK-dependent mechanism
Bin3
Methyltransferase Activity
Not required for 7SK stability or function
Hexim
Bin3
Larp7
Cdk9
CycT
Kinase Activity
RNAPII transcription elongation repressed
(b) Tissue-specific, 7SK-independent mechanism
?
MSM
Bin3
?
MSM
Bin3
RNAPII transcription elongation repressed